p53 dynamically directs TFIID assembly on target gene promoters

Coleman, R. A.[1#], Qiao, Z. [1], Singh, S. K, [1]Peng, C. S.[1], Cianfrocco, M.[2], Zhang, Z.[3], Song, L.[1], Piasecka, A.[1], Aldeborgh, H.[1], Basishvili, G.[1], Rice, W.[4], and Liu, W. L.[1]

[1]Gruss-Lipper Biophotonics Center, Department of Anatomy and Structural Biology, Albert Einstein College of Medicine, Bronx, NY 10461, USA.

[2]Department of Cellular and Molecular Medicine, University of California, San Diego, La Jolla, CA 92093.

[3]Howard Hughes Medical Institute, Janelia Research Campus, Ashburn, VA 20147, USA.

[4]New York Structural Biology Center, 89 Convent Avenue, Manhattan, NY 10027

#To whom correspondence should be addressed. Department of Anatomy and Structural Biology, Albert Einstein College of Medicine, Bronx, NY 10461 Tel: 718-430-8623; Email: robert.coleman2@einstein.yu.edu

Running title: Dynamics and structure of p53-induced TFIID assembly

Keywords: p53; TFIID; transcription; structure; single molecule microscopy

Abstract

p53 is a central regulator in tumor suppression. In response to various signals, p53 turns on vast gene networks to maintain cellular integrity, in part by aiding promoter recruitment of the TFIID-mediated transcription machinery to stimulate transcription initiation. However, the precise means by which p53 dynamically interacts with TFIID to facilitate assembly on target gene promoters remains elusive. To address this key question, we have undertaken an integrated approach involving single molecule fluorescence microscopy, single particle cryo-electron microscopy, and biochemistry. Our real-time single molecule imaging demonstrated that p53 both delivers and promotes the stable binding of TFIID to DNA. Furthermore, TFIID binds core promoter sequences via distinct modes displaying transient and prolonged stability. Importantly, TFIID's interaction with DNA induces p53 to rapidly dissociate, effectively recycling p53's binding site on the promoter. This notion is further supported by our structural studies. In addition, upstream promoter DNA comprising p53's response elements is highly mobile when bound to TFIID compared to the core promoter DNA. Collectively, these findings indicate that p53 serves as an escort to dynamically recruit and load the basal transcription machinery onto its target promoters by regulating the structural architecture of TFIID.

66 **Introduction**

67

68 More than 50% of cancer patients harbor p53 mutations, highlighting the essential role of
69 this protein in tumor suppression (1). To properly maintain genomic stability, p53 induces vast
70 gene networks involved in diverse cellular pathways including cell cycle arrest, apoptosis and
71 DNA repair (2). In response to various stress stimuli, p53 acts as a transcriptional activator that
72 specifically binds consensus response elements (REs; two ten base-pair half sites,
73 RRRCWWGYYY) within its target genes to directly stimulate gene expression (2). p53's search
74 for target REs is potentially expedited by its ability to non-specifically bind and slide along the
75 DNA (3). Upon recognition of its response genes, p53 facilitates transcription at least in part by
76 targeting the TFIID-mediated transcription machinery to the promoter (4-7). This large TFIID
77 complex, composed of TBP and 14 TBP-associated factors (TAFs), is responsible for
78 recognizing and binding multiple specific regions of the promoter (i.e. core promoter elements)
79 surrounding the transcription start site (TSS) (8). Once bound, TFIID serves as a central scaffold
80 for basal factors, which include RNA Polymerase II, to form a pre-initiation complex (PIC) that
81 culminates with active transcription. Importantly, without the assistance of activators such as p53,
82 TFIID's recognition of core promoter DNA sequences is weak and rate limiting for transcription
83 initiation due to inefficient PIC assembly (9-16). As TFIID is responsible for transcription of at
84 least ~90% of protein-coding genes (17), unraveling how p53 intervenes in this central step of
85 the PIC assembly (i.e. TFIID's binding of promoter DNA) is essential for understanding
86 mechanisms controlling gene-specific transcription initiation throughout the cell.

87 Previous biochemical studies of different activators (e.g. p53 and Zta) suggested a
88 conserved albeit poorly characterized mechanism for facilitating transcription (10, 18, 19). It has
89 been shown that p53 binds to its REs and enhances TFIID promoter recruitment via direct

90 contact with TBP and select TAFs (19, 20). Each of the various p53 target genes has a unique
91 arrangement of REs and core promoter elements (e.g. the TATA box, Initiator, and downstream
92 core promoter elements [DPE] (8)), which exhibit varied affinities for p53 and TFIID,
93 respectively (1). It is unclear how the variable spatial arrangement of REs with respect to core
94 promoter elements leads to distinct PIC assembly dynamics and gene-specific
95 p53/TFIID/promoter DNA structures. Additional evidence has shown that p53 and other
96 activators also stimulate structural changes within TFIID when associated with TFIIA and DNA
97 (10, 18, 19). This activator-induced isomerization results in the enhanced ability of TFIID to
98 bind core promoter element sequences downstream of the TSS (10, 18, 19). However, the
99 structural mechanism of p53-induced isomerization of TFIID and its impact on PIC assembly is
100 currently unknown.

101 Single molecule/particle-based imaging has emerged as an advanced tool to study
102 complex dynamic behavior and static structures of large multi-subunit protein assemblies
103 involved in regulating gene expression. A recent study utilizing real-time single molecule
104 fluorescence microscopy provided insight that TFIID's interaction with a synthetic core
105 promoter DNA tightly correlates with productive transcription (21). Despite years of intense
106 studies, how activators regulate TFIID's dynamic binding to native target DNA remains elusive.
107 In addition, advanced single particle transmission electron microscopy (EM) has unraveled the
108 three-dimensional (3D) structures of TFIID and its co-complexes. Recent EM studies unmasked
109 a structural plasticity of TFIID, likely attributed to its promoter recognition activity (20, 22-25).
110 In particular, human TFIID features a "horseshoe" shape containing three major lobes (A, B &
111 C) and a well-defined central cavity (26, 27). Interestingly, we demonstrated that, in the absence
112 of DNA, three different activators (e.g. p53) introduce a common set of local structural changes

113 in TFIID, including movement of lobe A towards lobe B resulting in a more closed central cavity
114 (20). Intriguingly, it was recently discovered that human TFIID undergoes a significant structural
115 rearrangement involving movement of Lobe A when bound to a specific promoter DNA
116 optimized for TFIID recognition (24). Whether p53's induced movement of Lobe A results in a
117 rearranged conformation of TFIID that contributes to stable interaction between TFIID and DNA
118 remains to be determined.

119 To uncover the mechanistic underpinnings of how p53 dynamically facilitates TFIID
120 assembly on promoter DNA, we exploited a combination of biochemistry, single molecule
121 fluorescence microscopy and single particle cryo-EM analysis. These studies illuminate dynamic
122 interactions and static global molecular architectures of p53-induced TFIID assemblies on two
123 representative target genes (i.e. *hdm2* and *bax*). Our real-time single molecule studies reveal that
124 p53 transiently interacts with DNA to help load TFIID onto promoters. To assist recruitment,
125 p53 stimulates structural rearrangement of TFIID to allow anchoring of downstream core
126 promoter DNA sequences. Notably, binding of TFIID to DNA induces dissociation of p53 from
127 the promoter, thereby effectively "recycling" the RE to allow recruitment of additional factors
128 involved in PIC formation. Our cryo-EM analyses further support this finding. In addition, the
129 upstream promoter that contains p53's response elements exerts structural plasticity when bound
130 to TFIID while the core promoter is stably bound. Collectively, these studies suggest that proper
131 response to divergent stress signals involves conserved structural mechanisms relating to p53's
132 ability to dynamically stimulate TFIID's interaction with various target promoters.
133

133 **Results**

134 ***Characterization of p53's impact on TFIID/DNA binding***

135 We sought to decipher the molecular mechanism of how p53 targets TFIID to stimulate
136 transcription. To achieve this goal, we chose two representative p53 target genes, *bax* and *hdm2*
137 (28, 29). We previously established unique purification strategies to isolate stoichiometric
138 activator/TFIID assemblies with high purity and determined their 3D structures (20). Here our
139 protocol was adapted to include the addition of native promoter DNA fragments (i.e. *bax* or
140 *hdm2*, Figure 1). In brief, we conducted highly specific immunoprecipitations (IP) from
141 fractionated HeLa nuclear extracts using a monoclonal antibody (mAb) against the TAF4 subunit
142 of TFIID (Figure 1A). Resins containing the immunoprecipitated TFIID were washed
143 extensively and split into four reactions (as indicated in Figure 1A). Next, while TFIID was still
144 bound to the TAF4 affinity resin, three of these reactions were incubated with 1.) a 6-fold molar
145 excess of the native promoter DNA alone; 2.) promoter DNA and purified human p53; or 3.)
146 promoter DNA, p53 and TFIIA, respectively. Unbound factors and DNA were removed by
147 extensive washing of the TAF4 affinity resin. Co-complexes containing DNA and/or factors
148 bound to TFIID were eluted from the resin using specific peptides recognized by the TAF4 mAb.
149 The TFIID assemblies were analyzed by SDS-PAGE and silver staining (Figure 1B).

150 We found that addition of p53 increased the amount of promoter DNA fragments co-
151 purifying with TFIID (Figure 1B, lanes 3, 4, 9 and 10) compared to TFIID incubated with DNA
152 alone (lanes 2 and 8). These results suggest that p53 aids in TFIID's binding to native target
153 gene promoters. A previous biochemical report documented that p53 stimulated the assembly of
154 TFIIA and TFIID on a synthetic promoter DNA (19). Consistent with these observations,
155 addition of TFIIA along with p53 (lanes 4 and 10) further enhanced the amount of DNA co-

156 present with TFIID compared to incubation of p53 alone (lanes 3 and 9). Collectively, these
157 results suggest that p53 promotes TFIID binding to DNA.

158 ***p53 facilitates binding of TFIID to DNA via the response elements and core promoter***

159 We sought to further understand the molecular mechanism pertaining to TFIID's
160 enhanced DNA binding (Figure 1B). Thus, dynamic interactions between p53, TFIID and
161 promoter DNA were characterized via a single molecule co-localization assay using Total
162 Internal Reflection Fluorescence Microscopy (TIRF) (21) along with Quantum dot-labeled
163 TFIID (QD-TFIID) and Cy3/Cy5-labeled native promoter DNA templates (Figure 2A). 2D
164 Projection maps indicated weak binding of TFIID to DNA within the first 15' with only 1.3% of
165 the wild-type *hdm2* DNA occupied by TFIID (Figure 2B, left two panels). The majority of bound
166 complexes lasted ~7" (left two panels and Figure 3A), revealing a low intrinsic affinity of TFIID
167 for DNA. Increasing the time between addition of TFIID to the DNA and the imaging of binding
168 did not improve co-localization efficiencies (data not shown), suggesting that reactions are at
169 equilibrium. This finding suggests that, at low concentrations (~1nM), TFIID inefficiently
170 recognizes DNA. On the other hand, increased binding of TFIID to DNA was observed in our
171 bulk biochemical assembly assays when much higher concentrations (100-600nM) were used as
172 in Figure 1B.

173 Upon addition of p53, a clear enhancement of *bax* or *hdm2* promoter DNA bound by
174 TFIID was observed (Figure 2B, right panel and Figure 2C), which is consistent with the general
175 increase of DNA retained in our bulk biochemical assays (Figure 1B). This significant
176 enhancement is due to the direct interaction between p53 and TFIID, because a control
177 experiment detected no p53-mediated co-localization of DNA with the Quantum dot-labeled

178 TAF1 antibody (0.2 ± 0.07% co-localization) in the absence of TFIID (data not shown). These
179 results confirm that p53 greatly facilitates TFIID binding to DNA.

180 To address the role of the p53 RE and core promoter elements in p53-mediated
181 TFIID/DNA binding, three mutant *hdm2* DNA templates were analyzed with the same real-time
182 co-localization assay (Figure 2C). The first mutant *hdm2* DNA template (i.e. Mu RE) harbors
183 mutations in the response elements known to impair p53's sequence-specific interactions (30). A
184 mild decrease of TFIID/DNA binding was observed on the mutant p53 RE template (Figure 2C).
185 This result suggests that p53's direct contacts with its RE are not critical for enhanced
186 TFIID/promoter DNA binding and other mechanisms may be utilized. Next, to assess the impact
187 of the core promoter in p53-mediated TFIID/DNA binding, mutations (i.e. Mutant Core) known
188 to inhibit transcription (31) were exploited. Upon addition of p53, TFIID's binding to the mutant
189 core promoter was reduced (Figure 2C). When both the p53 RE and core promoter elements
190 were altered (i.e. Mu p53 RE/Core), TFIID/DNA co-localization was significantly decreased
191 compared to the wild-type promoter (Figure 2C). These results indicate that the p53 RE and core
192 promoter elements were both required for optimal interaction of TFIID with p53 target gene
193 promoters.

194 As an alternative approach to study p53-mediated TFIID/DNA binding, we developed an
195 in vitro formaldehyde-crosslinking/exonuclease mapping assay (xlink-Exo), adapted from a well-
196 established strategy (ChIP-exo) to map out protein/DNA contacts of transcription factors in vivo
197 at near base-pair resolution (32). This analysis revealed that TFIID made extensive contacts with
198 well-characterized core promoter elements (i.e. TATA, InR, MTE and DPE) on the wild-type
199 *hdm2* DNA (Figure 2D, top panels). Notably, addition of p53 led to elevated crosslinking of
200 TFIID to the wild-type core promoter with select elements showing much larger changes (i.e.

201 TATA, InR) than others (i.e. MTE/DPE) (top panels). This result is consistent with our single
202 molecule data showing that p53 increases the specific binding of TFIID to the core promoter.
203 Importantly, when the Mu RE/Co and Mu Core templates were examined, a clear reduction in
204 p53's ability to selectively enhance contacts within mutated core promoter elements was
205 observed (Figure 2D, bottom panels and Supplemental Figure S1). This finding suggests that a
206 reduction of p53-mediated TFIID contacts within TATA, InR and the DPE leads to a decrease
207 co-localization of TFIID with mutant promoters (Figure 2C). TFIID's contacts within the -4 and
208 +11 regions were still slightly elevated in the presence of p53 on these mutant core promoters.
209 This result may explain why some percentage of TFIID/mutant DNA co-localization was
210 retained in our single molecule assays (Figure 2C).

211 In addition to these well-established contacts, previous DNAse I footprinting studies
212 reported TFIID/DNA interactions downstream of the DPE (+32 to +68) and upstream of TATA
213 (-40 to -140) (24, 33, 34). Our xlink-Exo assays also mapped TFIID/DNA interactions far
214 upstream of TATA (-55 to -137) and downstream of the DPE (~ +37 to +68), which were
215 enhanced when p53 was co-present on the wild-type *hdm2* promoter (Figure 2D). Therefore,
216 TFIID may utilize additional uncharacterized elements to recognize promoters. Surprisingly,
217 some of TFIID's upstream contacts (i.e. -55, -61, -80, and -88) reside within the p53 RE on the
218 wild-type promoter even in the absence of p53 (Figure 2D, top panels). Mutations of the p53 RE
219 led to a loss of TFIID's contacts at -61 and -88, indicating that TFIID recognizes specific
220 sequences within the p53 RE (Figure 2D bottom panels and Supplemental Figure S1).

221 ***p53 stabilizes TFIID binding at the core promoter***

222 Thus far, our studies demonstrate that p53 stimulates the association of TFIID with
223 promoter DNA. To test if p53 could also stabilize TFIID's binding to DNA, the amount of time

224 that QD-TFIID remains bound to a single promoter DNA before dissociating (i.e. residence time)
225 was determined (Figures 3 and Supplemental Figure S2). In the absence of p53, two populations
226 of DNA-bound TFIID complexes displaying distinct residence times were detected on the wild-
227 type *hdm2* template (i.e. long- and short-lived binding events) (Figure 3A, left panel).
228 TFIID/DNA binding events were predominantly short-lived (average residence time of 7.1 ± 0.6
229 seconds), with a minority of long-lived events (68.4 ± 8.0 seconds). Importantly, when p53 was
230 present, a majority of TFIID complexes on the wild-type *hdm2* DNA switched to long-lived with
231 an average residence time of 99.8 ± 5.0 seconds, while a minority exhibited a short-lived
232 residence time of 12.2 ± 0.8 seconds (right panel). TFIID also displayed a similar stability on the
233 *bax* promoter in the presence of p53 (Supplemental Figure S3). These results suggest that TFIID
234 alone weakly interacts with the DNA via two intrinsic binding modes that are both stabilized
235 when p53 is added.

236 We next assessed the role of the RE and core promoter elements in p53-mediated
237 stabilization of TFIID on DNA. Interestingly, disruption of the p53 binding site on the *hdm2*
238 promoter (Mu p53 RE) predominantly reduced the long-lived residence time of TFIID (avg =
239 75.1 ± 5.6") without significantly affecting the short-lived events (avg = 11.6 ± 1.0") (Figure 3B,
240 left panel). This suggests that interactions between p53 and its RE are required for maximal
241 stability of TFIID/DNA contacts on native target promoters. On the mutant core promoter (Mu
242 Core), a slight majority of TFIID/DNA binding events was now short-lived (54%). Residence
243 times for both the long- and short-lived TFIID/DNA binding events were also reduced (i.e. avg =
244 63.3 ± 4.7" and 5.8 ± 0.4", center panel), suggesting that both DNA binding modes were related
245 to core promoter recognition. When both the p53 RE and core promoter were altered (Mu
246 RE/Co), TFIID's promoter binding events were predominantly short-lived (72%) with reduced

247 short- and long-lived residence times relative to wild-type DNA (compare Figure 3B, right panel
248 v.s. Figure 3A, right panel). These experiments demonstrate that mutations of select core
249 promoter elements result in reduced stability of TFIID on DNA with additional changes in the
250 p53 RE further weakening its binding. Interestingly, our xlink-Exo studies showed that only a
251 few TFIID contacts on the mutant Core and RE/Core templates were slightly enhanced by p53
252 (Figures 2D and S1). Together with the single molecule data, our studies suggest that these
253 remaining enhanced contacts are sufficient to anchor TFIID, albeit weakly, to DNA. Overall,
254 these studies indicate that p53 generally enhances the stability of TFIID on DNA, which could be
255 important for recognition of weak non-consensus core promoter elements within p53 target genes.
256 Optimal stability requires p53's stimulation of TFIID's interaction with both the core promoter
257 elements and p53's binding site.

258 ***TFIID alters the binding dynamics of p53 to its cognate sites***

259 Our previous study revealed that a variant form of TFIID could cooperatively increase
260 the binding of the activator c-Jun to its binding site on promoter DNA (22). To quantitatively
261 assess if this was the case for p53, the dissociation dynamics of fluorescently labeled-p53/DNA
262 interactions plus or minus TFIID were examined (Figure 4). In the absence of TFIID, p53
263 primarily displayed two populations of distinct binding events on the wild-type *hdm2* template
264 (i.e. long-lived [avg = 33.1 ± 3.9"] and short-lived [avg = 7.4 ± 0.7"], Figure 4A, left panel).
265 Since earlier reports showed that p53 can bind DNA non-specifically (35, 36), we hypothesized
266 that these short-lived p53/DNA binding events were non-specific interactions. To test our
267 hypothesis, the same experiments were performed using the mutant p53 RE template (right
268 panel). Indeed, disruption of p53's sequence-specific binding sties on DNA led to a single short-
269 lived population (avg = 6.8 ± 0.7"). Based upon this result, the long-lived p53/DNA binding

270 events most likely represent sequence-specific interactions (left panel), whereas the short-lived
271 p53/DNA binding events are non-specific in nature. Alternatively, these short-lived events could
272 represent interactions with an unknown lower affinity p53 binding site in the promoter or binding
273 of dimeric p53 to consensus half-sites within the mutant RE. Notably, photobleaching of the
274 fluorescently labeled p53 did not affect our results, since similar residence times were observed
275 with multiple dyes of differing photostability (data not shown). In addition, a previous study
276 detected similar short residence times of ~10-12" for p53 bound to a consensus site (37).
277 Collectively, these results indicate that p53 dynamically interacts with DNA via both specific
278 and non-specific interactions.

279 Intriguingly, addition of TFIID resulted in a single population of p53 bound to wild-type
280 DNA with an "intermediate-lived" residence time distinct from the two populations observed
281 with p53 alone (Figure 4B). We noticed that fitting of the data showed slight deviations from an
282 exponential decay model. Importantly, a previous study indicated that the existence of complex
283 multi-step dissociation events could be discerned using a gamma distribution model to fit single
284 molecule data (38). Indeed, the data was better represented by a gamma distribution model (right
285 panel). Parameters from the gamma distribution fit reveal that, in the presence of TFIID, p53
286 dissociates from the DNA in ~2 steps with roughly equivalent residence times of 8.2" per step
287 (average total time = 14.8 ± 1.5"). Furthermore, gamma distribution fitting of p53's dissociation
288 from wild-type DNA in the absence of TFIID indicated a single step dissociation pathway (data
289 not shown). These findings demonstrate that TFIID alters both the rate and mechanism of p53's
290 dissociation from promoter DNA.

291 Given that TFIID directly contacts the RE as revealed via our xlink-Exo assays (Figure
292 2D, top panels), it is possible that TFIID could help stabilize p53 binding to weak REs. Indeed,

293 in the presence of TFIID, there was a slight enhancement of p53's residence time on the Mu RE
294 DNA compared to p53 alone (Supplemental Figure S4A left panel versus Figure 4A right panel),
295 consistent with TFIID stabilizing p53's binding to a non-canonical mutant RE. This subtle
296 stabilization does not require TFIID's interaction with the TATA, InR and DPE elements, since
297 we also observed an increase in p53's residence time on the Mu RE/Co DNA (Supplemental
298 Figure S4B). Fitting of the dissociation data on the mutant templates to a gamma distribution
299 yielded poor fits, suggesting single step dissociation kinetics despite fitting parameters that
300 indicated a multi-step dissociation (Figures S4, right panels). Overall, these data indicate that
301 TFIID binding to DNA can influence p53's stability at the RE. TFIID's interaction with p53
302 likely promotes the dissociation of p53 bound to specific sequences in the promoter. Importantly,
303 the average time of p53 bound to the wild-type *hdm2* template (~15") is significantly shorter
304 than TFIID's long-lived DNA binding time (~100") (Figure 4C). These dynamic studies strongly
305 suggest that p53 transiently escorts TFIID to the promoter DNA. Importantly, p53 is not required
306 to remain bound for TFIID's maximum stability on promoter DNA.

307 ***p53 promotes a common DNA binding conformation of TFIID***

308 Since p53 enhances TFIID's binding to DNA, we speculated that p53 regulates the
309 structural architecture of TFIID to aid recognition of various target genes. Our previous
310 structural studies demonstrated that, in the absence of DNA, p53 binds TFIID via its direct
311 contact with Lobe A and C (20). Intriguingly, this p53-bound TFIID did not undergo drastic
312 conformational changes. Rather, the p53/TFIID interaction led to unique local structural changes
313 within TFIID including the movement of Lobe A towards Lobe B (20). A recent cryo-EM study
314 discovered that human TFIID switches from a canonical to a rearranged conformation that
315 permits binding to the super core promoter (SCP) DNA optimized for interaction with TFIID (24,

316 31). This rearranged DNA binding conformation of TFIID was formed by the movement of Lobe
317 A from Lobe C to Lobe B (24). It was previously unclear how this p53-induced Lobe A
318 movement toward Lobe B was related to TFIID's rearranged DNA binding conformation.
319 Therefore, we hypothesized that p53-induced local structural changes aid in formation of the
320 rearranged state to facilitate TFIID's interaction with DNA. To test this idea, we set out to reveal
321 TFIID's global structural architecture when p53 and target promoter DNA were present.

322 As the first step, unbiased reference-free 2D classification experiments were performed to
323 examine conformational states of TFIID when p53 alone and p53/*bax* DNA were present (Figure
324 5A). Three conformational states of TFIID represented by corresponding views of 2D class
325 averages were classified based upon the position of Lobe A relative to Lobes C and B (top panels,
326 i.e. canonical, transition, and rearranged state). Strikingly, in the presence of p53, an elevated
327 population of TFIID displayed the rearranged form, while the percentage of transition state
328 remained similar compared to TFIID alone (bottom panel). This finding suggests that p53 can
329 specifically impact formation of TFIID's rearranged state. To assess the effect when p53 and the
330 *bax* DNA were added, the same 2D classification analysis was also conducted. Interestingly, the
331 populations of both the transition and rearranged forms increased when p53 and DNA was co-
332 present (bottom panel). This observation indicates that target gene promoters and/or its
333 interaction with p53 also play a role in TFIID's conformational switches.

334 A previous biochemical study reported that p53 stimulated the assembly of TFIIA and
335 TFIID on a synthetic promoter DNA (19). Interestingly, unlike p53, TFIIA alone promotes the
336 canonical form of TFIID (24). Thus, to assess p53's impact on the structural framework of
337 TFIID in the presence of TFIIA, two TFIID/p53/TFIIA assemblies on the native *hdm2* and *bax*
338 promoter fragments (488 bp and 500 bp) were obtained as described in Figure 1 (Supplemental

339 Figure S5). To visualize both conformations and the DNA, cryo-EM data of these assemblies
340 were collected for reference-free 2D classification analysis. Some class averages showing the
341 presence of promoter DNA spanning the central cavity of TFIID were observed (Figure 5B).
342 Surprisingly, both assemblies displayed a similar rearranged TFIID architecture, despite the
343 different organization of their promoters. Each template harbors non-canonical core promoter
344 elements with different spatial arrangements between TATA and the Initiator (Figure 1B) (8, 28,
345 39). Combined with our 2D classification analysis (Figure 5A), these structural studies suggest
346 that p53 promotes formation of a common rearranged TFIID/DNA binding conformation.

347 Next, to identify the relative DNA orientation and any distinct structural features, we
348 compared the class averages of our two assemblies with the previous structural analysis of
349 TFIID/TFIIA/SCP DNA containing a mapped DNA orientation (24). Our co-complexes
350 displayed clear views of TFIID stably bound to the *bax* DNA downstream of the TSS (Figure 5C,
351 top two panels). In contrast, upstream promoter DNA was weakly visible in our averages
352 (middle panel). These results suggest that the p53 RE upstream of the TATA box element is
353 flexible within the co-complex. To define the presence of the upstream promoter, focused
354 classification on a class average displaying flexible upstream DNA (middle panel) was
355 performed as previously described (24). This analysis revealed a clear density for the upstream
356 promoter DNA (highlighted by yellow arrow, bottom panel). Given the strong density for
357 downstream DNA within the assembly, these results indicate that TFIID serves as a strong
358 anchor for downstream promoter DNA during PIC assembly.

359 Another observation is that the 2D class averages of p53/TFIID/TFIIA/DNA assemblies
360 exhibit a similar topology to the averages from TFIID/TFIIA bound to the SCP DNA (refer to
361 Figure 3 in (24)) raising two major points. First, these data suggest that TFIID adapts a common

362 DNA binding conformation to bind various p53 target gene promoters. Second, p53 may
363 dissociate from TFIID, as supported by our single molecule dynamics results (Figure 4), in order
364 to complete structural rearrangements associated with the DNA binding form of TFIID. To test
365 these hypotheses, single particle 3D reconstruction was conducted to determine the 3D structure
366 of the TFIID/TFIIA/p53/*bax* DNA co-complex (Supplemental Figure S6A). The overall
367 structural architecture of our co-complex is comparable to the 3D structure of TFIID/TFIIA/SCP
368 DNA. Our 3D reconstruction was also verified by analyzing its 3D projections with their
369 matching reference-free 2D averages (Supplemental Figure S6B). This result suggests that TFIID
370 utilizes one common rearranged form to bind various promoters.

371 Our 3D reconstruction did not reveal any prominent extra densities that would most
372 likely represent the p53 protein. This indeed suggests that either p53 dissociates from the
373 TFIID/TFIIA/*bax* DNA co-complex or p53 has a transient interaction with the assembly, which
374 led to the EM density being averaged out during analysis. The same observation was also
375 obtained with the 3D structure of the TFIID/TFIIA/p53/*hdm2* promoter DNA (Supplemental
376 Figure S7). Since we previously determined the 3D structure of the p53 bound TFIID co-
377 complex without DNA (20), we attempted to capture the p53-bound state of TFIID in the cryo-
378 EM dataset of our TFIID/TFIIA/p53/*bax* DNA assembly. Thus, 3D reconstructions were
379 performed using the structure of p53/TFIID as an initial reference volume. A poor resolution 3D
380 reconstruction of p53/TFIID was obtained (Supplemental Figure S8), indicating that the majority
381 of TFIID complexes have switched to the p53-free DNA-bound state. Collectively, these
382 structural studies support the observations from our single molecule analyses, illustrating that
383 p53 dissociates from TFIID and DNA when recruited to target promoters. More importantly, our
384 work suggest that p53 facilitates the formation of a common rearranged DNA binding

385 conformation of TFIID to stimulate promoter recruitment on various target genes.

386

386 **Discussion**

387 ***p53 promotes distinct DNA binding modes within TFIID***

388 p53-mediated binding of TFIID to promoter DNA is likely a multi-step process involving
389 the formation of multiple coordinate contacts between p53, the RE, TFIID and the individual
390 core promoter elements. Our single molecule analyses strongly suggest that p53/TFIID interacts
391 with target gene promoter DNA via two distinct DNA binding modes with a strong preference
392 for stable binding over transient interaction. Remarkably, TFIID's DNA binding mechanism
393 appears to be similar on the *hdm2* and *bax* DNA, despite different spatial arrangements and
394 sequences in the p53 RE and core promoter elements. It would be interesting to determine if
395 TFIID's residence time on DNA is dependent on the type of activator utilized to load TFIID onto
396 the promoter and how this correlates with the frequency of transcription initiation/re-initiation.

397 To potentially address how TFIID engages promoter DNA differentially, we studied how
398 these two populations of DNA-bound TFIID complexes responded to mutations in the core
399 promoter elements and the p53 RE. Intriguingly, the majority of DNA binding events on the
400 mutant core promoters were short-lived (Figure 3B). Residence times for both the long- and
401 short-lived TFIID complexes were also reduced. TFIID's decreased stability is likely due to
402 changes in contacts with the TATA, InR, and DPE on the Mu Core DNA as revealed in our
403 xlink-Exo assays (Figures 2D and S1). Strikingly, mutation of the p53 RE primarily affected the
404 residence time of TFIID's long-lived DNA binding population (Figure 3B). This finding suggest
405 that contacts between p53 and the RE are somehow required to increase the stability of TFIID on
406 promoter DNA via an unknown mechanism. Given that distinct TFIID contacts surrounding the
407 p53 RE were identified via our xlink-Exo assays (Figure 2D), we speculate that this upstream
408 DNA is involved in both binding p53 and stabilizing TFIID to the promoter. These upstream

409 contacts may be possibly mediated by the TAF4 subunit of TFIID, which was previously shown
410 to bind ~70 bp of DNA with a weak sequence preference (40).

411 Thus far, we surmise that TFIID/DNA binding occurs through at least two discernable
412 regulatory steps involving recognition of multiple different core promoter elements. The short-
413 lived DNA binding population could likely represent a transient non-productive TFIID complex,
414 which initially encounters the promoter DNA and is only partially engaged with the core
415 promoter elements (Figure 6). In such a scenario, interaction between p53 and its RE promotes
416 efficient isomerization within the initial TFIID/DNA encounter complex. This p53-mediated
417 isomerization step may possibly permit stable interaction of TFIID with the upstream DNA,
418 TATA box and downstream DNA resulting in long-lived DNA binding (Figure 6), which is
419 consistent with our xlink-Exo data (Figure 2D). In support of this model, previous biochemical
420 assays have shown that activators induce conformational changes within TFIID that enhance
421 multiple contacts with promoter sequences downstream of the TSS (10).

422 ***TFIID switches p53 to a factor-loading mode to "recycle" the p53 RE***

423 In the absence of TFIID, p53 displays both specific and non-specific DNA binding modes
424 (i.e. average residence time = ~33" and ~7"). Remarkably, TFIID's presence switches p53 to a
425 single "factor-loading" mode with a residence time on DNA (~15") that is intermediate to its
426 specific (~33") and non-specific rates (~7") (Figure 4). A previous study documented that p53
427 binds non-specific DNA via select residues in its lysine rich C-terminal domain (CTD) (36).
428 Interestingly, TFIID's TAF1 bromodomains interact with acetylated marks on many of these
429 same residues in p53's CTD (41). Therefore, it is possible that TFIID's interaction could
430 eliminate p53's short-lived (7") population by sterically hindering its ability to non-specifically
431 bind DNA. Strikingly, deletion of the CTD also allosterically reduces p53's binding to specific

432 DNA targets (42, 43). Thus, we speculate that the interaction between TFIID and the CTD of
433 p53 would also explain the reduction in the long-lived residence time of p53 on specific DNA
434 sites. Overall, TFIID potentially alters p53's DNA binding dynamics by eliminating non-specific
435 DNA binding, reducing the affinity of p53 for specific target sites via contacts within its CTD,
436 and sterically blocking p53's contacts with specific DNA residues via direct TAF contacts within
437 the RE.

438 Our results show that TFIID's DNA binding induces dismounting of p53 from the
439 promoter, consistent with previous DNAse I footprinting studies showing decreased binding of
440 p53 to REs in the presence of TFIID (19). While p53 dissociates from the TFIID/DNA scaffold,
441 it is highly likely that p53 can rapidly re-associate with the complex, particularly at the high
442 concentrations (600nM) used in Figure 1B. We suspect that this rapid removal could
443 consequently lead to a faster "recycling" of p53 from the RE for its subsequent recruitment of
444 other basal transcription factors such as TFIIB (44, 45) and TFIIH (46-48). In this scenario,
445 stable prolonged binding of p53 to a TFIID/DNA complex would negatively regulate PIC
446 formation, because p53 would occupy the RE and inhibit subsequent recruitment of a p53/basal
447 factor co-complex. Notably, the residence times for p53 and TFIID at the promoter were
448 measured in the absence of additional PIC components. Most likely, additional factors such as
449 TFIIA, TFIIF, and RNA Polymerase II will alter the stability of TFIID and p53 as the PIC forms
450 on promoter DNA. Indeed, our previous single molecule studies showed prolonged binding of
451 QD-TFIID to DNA in the presence of PIC components (21). This suggests that our current work
452 here measures TFIID dissociation events and not simply dissociation of the QD labeled TAF1
453 antibody. Overall, our studies indicate that p53, and potentially activators in general, serve as

454 escorts to dynamically recruit and load the basal transcription machinery onto DNA via complex
455 interactions between the RE, the core promoter and bound basal factors (i.e. TFIID).

456 ***p53 facilitates formation of a common rearranged DNA binding framework of TFIID***

457 Our previous structural studies demonstrated that, in the absence of DNA, p53 bridges
458 TFIID's Lobe A/C while introducing movement of Lobe A towards Lobe B (20). Interestingly,
459 repositioning of Lobe A to Lobe B is a hallmark feature associated with a rearranged form of
460 TFIID that binds promoter DNA (24). Here we found that p53 and DNA enhances formation of
461 the rearranged TFIID via 2D classification analysis (Figure 5A). In addition, the majority of our
462 TFIID assemblies in the cryo-EM datasets display this rearranged DNA binding form (Figures 5
463 and S6). Therefore, these results strongly suggest that the p53-induced specific movement of
464 Lobe A within TFIID likely helps formation of a TFIID/DNA co-complex by shortening the
465 distance required for repositioning of lobe A to lobe B (24). In addition, we have determined that
466 the stable TFIID/DNA interaction does not require p53 to remain bound to TFIID and DNA
467 (Figures 4, 5 and S6). It is thereby reasonable to propose that p53 stimulates the transition of
468 canonical TFIID to the rearranged DNA binding state, followed by dissociation of p53 once
469 TFIID stably loads onto DNA (Figure 6).

470 Our single molecule studies indicate that p53 promotes both transient and stable binding
471 of TFIID to DNA. Due to this transient dynamic interaction behavior, we were likely unable to
472 obtain the 3D structure of those short-lived DNA-bound TFIID complexes via cryo-EM. It is
473 possible that these short-lived DNA-bound TFIID complexes could be a unstable "encounter
474 complex" (Figure 6) or reminiscent of the "recruitment" form of DNA-bound yeast TFIID
475 induced by the Rap1 activator in the absence of TFIIA (23). We speculate that the long-lived

476 DNA-bound TFIID complex induced by p53 is structurally related to the stable
477 TFIID/TFIIA/promoter DNA complex depicted in our cryo-EM studies.

478 Our cryo-EM analysis uncovers the global similarity of the 3D reconstructions between
479 p53/TFIID/TFIIA/*bax* DNA, p53/TFIID/TFIIA/*hdm2* DNA and TFIID/TFIIA/SCP DNA
480 (Figures 5B, S6 and S7). This significant observation in combination with our 2D classification
481 analysis (Figure 5A) clearly suggests that p53 aids in formation of a common DNA binding
482 mode of TFIID, which effectively allows TFIID to bind diverse target gene promoters.
483 Interestingly, p53 alone enhances the rearranged form of TFIID (Figure 5A), while TFIIA alone
484 promotes the canonical form (24). These observations indicate that different transcription factors
485 use distinct modes of structural regulation to stimulate TFIID recruitment. Nevertheless, it is
486 difficult to clearly define the individual roles of p53 and TFIIA in our 3D structures, because
487 each factor plus DNA is capable of promoting TFIID's rearranged DNA binding conformation
488 (this study and (24)).

489 Intriguingly, the proximal promoter DNA upstream of the TATA box is highly mobile
490 when TFIID binds to p53 target gene promoters as revealed in our 2D class average analysis
491 (Figure 5B). Notably, our sensitive xlink-exo assays were able to detect TFIID contacts with
492 upstream sequences (Figure 2D). These results suggest a dynamic transient interaction between
493 TFIID and upstream DNA. Since a number of activator binding sites reside in a promoter
494 proximal region upstream of the TATA box (49), our findings indicate the potential for TFIID to
495 also influence binding of other activators with their cognate sites as observed previously (22).
496 Collectively, our work reveals the molecular mechanism pertaining to how p53 stimulates TFIID
497 binding to different promoters that comprise variable arrangements of p53 binding sites and core
498 promoter elements. More importantly, our combined functional and structural studies are crucial

499 for understanding how eukaryotic transcription complexes dynamically assemble on different

500 protein-coding gene promoters.

501
502

502 **Materials and Methods**
503
504 **Reagents and protein purification**
505
506 Experimental details, including reagents, protein purification of the p53/TFIID/TFIIA/DNA
507 co-complexes and fluorescent-labeled proteins/DNA used in this study along with our custom-
508 built TIRF microscope setup, are described in the Supplemental Materials.

509 **In vitro immuno-assembly assay**

510 HeLa cells (32 liters) were grown in suspension culture with 1X DMEM plus 5% newborn calf
511 serum for each assay. Nuclear extract was prepared and fractionated with phosphocellulose P11
512 (P-Cell) resins exactly as previously described (20). P-Cell column fractions eluting at 1M
513 KCl/HEMG buffer (pH 7.9, [20 mM Hepes, 0.2 mM EDTA, 2 mM $MgCl_2$, 10% Glycerol, 1 mM
514 DTT and 0.5 mM PMSF]) were pooled, dialyzed to 0.3 M KCl/HEMG buffer, added with final
515 concentration of 0.1% NP40, and then immunoprecipitated overnight at 4°C with an anti-TAF4
516 mAb covalently conjugated to Protein G Sepharose beads (GE Healthcare Life Sciences). TAF4-
517 immunoprecipitates were extensively washed with 0.65 M KCl/HEMG buffer, 0.3 M
518 KCl/HEMG buffer and 0.1M KCl/HEMG buffer (containing 0.05% NP40 buffer and 10 μM
519 Leupeptin) and split into four assembly reactions as indicated in Figure 1. Three reactions of
520 TFIID-bound resins were incubated with 6-fold molar excess of promoter DNA. Next, two
521 TFIID/DNA reactions were further added with 10-fold molar excess of p53 alone and/or TFIIA.
522 Total four reactions were incubated at 4°C for 2 hours prior to elution of the co-complex from
523 the TAF4 mAb affinity resin. TFIID/factor/DNA-bound resins were washed 5 times with 0.1 M
524 KCl/HEMG buffer (containing 0.1% NP40 and 10 μM Leupeptin) followed by elution with a
525 peptide (1 mg/ml) in 0.1 M KCl/HEMG buffer (plus 0.1% NP40 and 10 μM Leupeptin)
526 recognized by the TAF4 mAb. Eluates were analyzed with 4-12% SDS-PAGE (NuPage gel

527 system, Thermo Fisher) and visualized with silver staining analysis.

528

529 **Xlink-Exo assay**

530 Xlink-Exonuclease assays were carried out in 10 µl reactions containing a modified 50 mM
531 KCl/HEMG buffer (pH 7.9, [12.5 mM Hepes, 0.05 mM EDTA, 6.25 mM $MgCl_2$, 5% glycerol]
532 plus 1% DTT, 0.05 M PMSF, and 0.01% NP-40), IRdye800 (IDT) antisense strand labeled *hdm2*
533 promoter DNA (9nM) , p53 (90nM, monomer), and TFIID (4nM). After incubation at room
534 temperature for 20', reactions were crosslinked with formaldehyde (1% final) for 5' and stopped
535 by addition of Tris-HCl (100 mM final, pH 8.0). Next, each reaction was mixed with
536 Exonuclease III (50 Units, NEB diluted in a buffer containing $MgCl_2$ [16.25 mM final]), and
537 incubated at 37°C for 1 hour. Proteinase K (10 µg) was then added into each reaction and
538 incubated at 70°C for 3 hours. Reactions were mixed in formamide loading dye, heated at 95°C
539 and resolved on a 8% Polyacrylamide-TBE gel containing 7M urea. A series of known 5'
540 truncated IRdye800 (IDT) antisense strand labeled wild-type *hdm2* DNA fragments were
541 generated and used as molecular standards to determine the size of Exonuclease III digested
542 bands seen on our mapping gels.

543

544 **TIRF Single Molecule Imaging**

545 Passivated glass coverslips (see Supplemental materials) were assembled into a multichannel
546 flow cell using double sided tape (3M). Flow cells were mounted on the microscope and
547 streptavidin was added to the flow cell to coat surfaces. Each flow cell holds ~50 ul of sample.
548 Reference beads that serve as fiducial marks were immobilized on the bottom surface of the flow
549 cell. Biotinylated Cy3/Cy5 promoter DNA in 1X PBS was then loaded into the flow cell and

550 bound over time specifically to the streptavidin that was non-covalently attached through biotin
551 linkages on the top and bottom surfaces. Promoter DNA templates were briefly imaged at 3HZ to
552 determine surface attached DNA densities that were sufficient for localization of single DNA
553 molecules. Unbound biotinylated Cy3/Cy5 promoter DNA was washed away. Promoter DNA
554 templates were then imaged at 3HZ. The surface attached Cy3/Cy5 promoter DNA was then
555 photobleached. Reactivation of the Cy3/Cy5-labeled promoter DNA was not evident over the
556 timescale of our experiments (typically 15-20 minutes). Qdot 565-labeled TFIID (1 nM) in the
557 absence and presence of unlabeled p53 (8 nM, monomer) was then added to the flow cell in a
558 modified 50 mM KCl/HEMG buffer (pH 7.9, [12.5 mM Hepes, 0.05 mM EDTA, 6.25 mM
559 $MgCl_2$, 5% glycerol] plus 1% DTT, 0.05 M PMSF, and 0.01% NP-40) and immediately imaged
560 at 3Hz at 23°C. An oxygen scavenging system consisting of 0.4% b-D-Glucose, 1 mg/ml glucose
561 oxidase (Sigma), and 0.4 mg/ml catalase (Sigma) was used for imaging. For experiments to
562 measure p53's interaction with promoter DNA, AlexaFluor 555, Cy3- or Cy5-labeled p53 (8nM,
563 monomer) in the absence or presence of unlabeled TFIID (1 nM) was added to the flow cell
564 containing surfaced attached mapped promoter DNA and immediately imaged at 3Hz.
565 AlexaFluor 555, Cy3- and Cy5-labeled p53 had equivalent residence times on promoter DNA
566 indicating that photobleaching of molecules didn't significantly affect results.
567
568 **Single Molecule Co-localization Analysis**
569 Fluorescent spots in each frame for the movie of the promoter DNA, TFIID or p53 were mapped
570 using 2D Gaussian fitting methods (21, 50, 51) to determine the location (x, y) at subpixel
571 resolution. Co-localization analysis was performed as in (21) with the following modifications.
572 Coordinates of fluorescent spots were adjusted based upon movement of the fiducial marks (i.e.
573 reference beads) over time. Stage movement/drift was typically less than 200 nm over the time of

imaging (~20 minutes). Fluorescent spots that were located within 84 nm (1 pixel) throughout the movie were grouped together in a cluster. The positions of all spots within a cluster were averaged to obtain the overall location of an individual cluster of molecules. Position maps of the clustered surface attached DNA molecules were then compared with position maps of either the TFIID or p53 clusters. Clusters of TFIID or p53 molecules within 3 pixels (252 nm) of a DNA cluster were found. Displacements of TFIID or p53 clustered molecules with a maximum equal to (0,0) in the x and y positions are indicative of non-random co-localization between DNA and TFIID or p53 clusters. Displacements between the x,y positions of the TFIID or p53 clusters and the DNA clusters were then plotted as a 2D histogram with a bin size of 50 nm. 2D Gaussian fitting of the 2D histogram yields σ which is equivalent to the variation in the displacement of TFIID or p53 within 252 nm of a DNA molecule. A co-localization threshold was set to 1.8σ (84 nm).

Single Molecule Residence Time Analysis of TFIID and p53 on promoter DNA

For each TFIID or p53 cluster that co-localized with a DNA cluster (i.e. within 84 nm), we the plotted the amplitude from the 2D Gaussian fit of every fluorescent spot within the TFIID or p53 cluster as a function of time. Homemade MATLAB software was then used to analyze the rise and the fall of the amplitude of the fluorescent signal to determine the appearance and corresponding disappearance of each spot over time. The residence time for each DNA binding event is defined as the difference in time between the appearance and disappearance of a TFIID or p53 fluorescent spot. The fluorescent signal from TFIID or p53 had to last for at least 1.5” to be considered as a discrete binding event in our analysis. Due to rapid stochastic blinking of the quantum dot, a dissociation event was only considered to have occurred if the quantum dot signal

597 remained in the off state longer than 4.5". At least 300 binding events of co-localized TFIID or
598 100 binding events of p53 clusters were analyzed for each particular promoter DNA construct.
599 For a subset of molecules (~100), the data was processed by hand to determine the appearance
600 and disappearance of fluorescent spots. Comparison of the residence times generated by our
601 automated software and by hand yielded negligible differences. Histograms of residence times
602 for TFIID or p53 bound to promoter DNA were fit to a two-component exponential decay model
603 to determine the average residence time of TFIID or p53 bound to promoter DNA (51). If the
604 difference between the fitted residence times for each individual component in the two-
605 component model varied less than 20%, histograms were re-fitted using a single-component
606 exponential decay model (51). For Figures 4 and S3 data was additionally fit to a gamma
607 distribution (38) via custom MATLAB software.
608
609 **2D Classification Analysis of TFIID co-complexes via negative stain EM**
610 4 μL (10-20 ng in total amount) of fresh TFIID/p53/bax DNA assemblies in 0.1M
611 KCl/HEMG buffer (20mM HEPES, 0.2 mM EDTA, 2mM $MgCl_2$, 10% Glucose [final pH 7.9])
612 was applied directly onto a thin carbon film supported by holey carbon on a 400-mesh copper
613 grid (Pacific Grid tech.) for 3', which was freshly glow-discharged. After incubating the sample
614 on the grid for 3', the sample grid was stained in five successive 75 μL drops of 1% Uranyl
615 Formate.
616 The negative stain image data were collected with a Tecnai F20 TWIN transmission
617 electron microscope operating at 120 keV at a calibrated magnification of 62,000x with a
618 defocus range of -0.5μm to -2.5μm using a Tietz F416 (4K x 4K) CCD camera (resulting in a
619 2.82 A/pixel) under the dosage 39.98 e^-/Å. A total of 14,000 particles (for TFIID alone), 13,855

620 particles (for TFIID/p53), and 19262 particles (for TFIID/p53/bax DNA) were manually picked
621 using Boxer (EMAN; (52)). These particles were aligned and classified in a reference-free
622 fashion as previously described (22) for 8 iterations. The similar measurement of Lobe's A
623 position relative to the lobes B and C was employed as in (24). Based upon the position of Lobe
624 A in relation to Lobe C v.s. Lobe B (24), three conformational groups of TFIID were defined (i.e.
625 canonical, transition, and rearranged state) in this study. The canonical form is represented by
626 Lobe A retaining its attachment to Lobe C. The transition state is represented by Lobe A
627 beginning to detach and move in between Lobe C and B. The rearranged form is represented by
628 Lobe A reattaching to Lobe B. Next, individual classums from the 5th , 6th, 7th and 8th iteration
629 for each TFIID/p53 prep with or without the *bax* DNA were examined carefully to select 2D
630 class averages displaying views of these three conformational groups. The number of 2D
631 averages in each conformational form v.s. total averages was calculated to yield the percentage
632 of TFIID's three conformations in each TFIID/p53 prep with or without the *bax* DNA. Three
633 independent protein purifications and EM data acquisition/analysis were performed to obtain the
634 statistically significant standard deviation for the figure.
635
636 **Cryo-EM data collection and image analysis**
637 For cryo-EM sample grid preparation, a thin carbon film supported by a 400-mesh carbon-
638 thickened C-flat holey grid with hole diameter 1.2 μm/spacing 1.3 μm (CF-1.2/1.3-4C,
639 Protochips) was plasma cleaned for 2 min using Denton high-vacuum evaporator. The grid was
640 loaded into a Vitrobot (FEI) that was preset at 100% humidity at 4ºC for vitrification of our
641 samples. 3 μl (504~900 ng in total amount) of the p53/TFIID/TFIIA/DNA assemblies was

642 applied directly onto the grid, incubated for 2 min and then blotted for 6.5 sec prior to plunge-
643 frozen in liquid ethane.

644 Cryo-EM data were collected with a JEM-2100F transmission electron microscope (JEOL)
645 operated at 120 KeV and at a magnification of 50,000x with a defocus range of –2.5 μm to –4.5
646 μm. Digital micrographs were collected using a TEM 2048x 2048 CCD camera (TemCam-
647 F224HD, TVIPS) with a pixel size of 24 μm and a calibrated magnification of 84,037x (2.86
648 Å/pixel) under low-dose conditions (~13 e^- /Å) via the semi-automatic image acquisition
649 SerialEM software (53). Digital micrographs showed homogeneous particles in terms of lack of
650 aggregation and apparent integrity of the intact complexes.

651 Particles were manually selected using boxer (EMAN) (52) for an initial total of 32,275
652 particles from the p53/TFIID/TFIIA/*bax* DNA dataset and 22,070 particles from the
653 p53/TFIID/TFIIA/*hdm2* DNA dataset. The particles were then phase flipped using CTF-
654 estimated values determined by CTFFIND3(54) and extracted using SPIDER (System for
655 Processing of Image Data from Electron microscopy and Related fields (55)) to a particle
656 window size of 128 x 128 pixels (5.72 Å/pixel), following the protocol as described in (24). The
657 particles were then normalized prior to the following data analyses. Reference-free 2D class
658 averaging image analysis was performed using IMAGIC (56) following the procedure precisely
659 as described (20). Using these 2D class averages as templates, we automatically picked particles
660 from a larger cryo-EM dataset using Signature (57) embedded in the Appion image processing
661 platform (58). A final total of 59,632 particles for the p53/TFIID/TFIIA/*bax* DNA co-complex
662 was obtained, normalized, and low-pass band filtered to perform the 3D reconstruction using
663 SPIDER's multi-reference projection matching approach as previously described (27). Both
664 rearranged and canonical forms of TFIID/TFIIA/SCP DNA from Eletron Microscopy Data Bank

665 (accession number 10832 and 10834, respectively) were filtered to 60 Å as a reference for the
666 first cycle of projection matching. Different initial reference models including TFIID alone, p53-
667 bound TFIID or TFIIA-bound TFIID were also tested for model bias refinement. New 3D
668 volumes reconstructed from the data set were used as references for all subsequent cycles of
669 alignment (angular step sizes ranging from an initial 20° to a final 2°). The resolution throughout
670 the refinement was determined by the 0.5 cut-off in the Fourier shell correlation (FSC) curve.
671 The 3D structure of the p53/TFIID/TFIIA/bax assembly was filtered at a final resolution ~35 Å.
672 All the 3D reconstructions were represented as isodensity surfaces using the UCSF Chimera
673 package (59) developed by the Resource for Biocomputing, Visualization, and Informatics at the
674 University of California, San Francisco (supported by NIH NIGMS P41-GM103311).
675
676

Funding information

This study was supported by Einstein start up fund (Albert College of Medicine). Some of this work was performed at the Simons Electron Microscopy Center at the New York Structural Biology Center that is supported by a grant from the Simons Foundation (Grant Number: 349247) with additional support from: NIH S10 OD019994-01, the Agouron Institute (Grant Number: F00316), NIH S10 RR029300-01, NIH S10 RR017291-01, NYSTAR, and NIH C06 RR017528-01-CEM.

Acknowledgement

We specifically thank R. Tjian, S. Chu, and E. Nogales for their initial support of this study, S. Zheng for generating TAF4 mAb supernatant and HeLa cells, D. King for providing the TAF4 mAb elution peptide, A. Revyakin, A. Pertsinidis and S.R. Park for their help on initial stages of the single molecule microscopy, along with R. Henderson and D. Stokes for their technical advice critical for the cryo-EM work. We also thank S.M. Shenoy, J. Hargitai, J. Wang, S. Lenny, J. Greally and E. Eng for high performance computing cluster and cryo-EM technical support. We appreciate assistance from Einstein's AIF facility, especially F. P. Macaluso, L. Cummins and G. S. Perumal. We are grateful to M. Keogh and E. Nogales for critical comments of the manuscript. W. Liu is an affiliated member of the New York Structural Biology Center. M. Cianfrocco is an HHMI fellow of the Damon Runyon Cancer Research Foundation.

698 **Figure legends**

699 **Figure 1. In vitro assembly of p53/TFIID/TFIIA/promoter DNA complexes.** (A) Schematic
700 representation of procedures for assembly assays to study TFIID bound to p53, TFIIA and native
701 p53 target gene promoter DNAs in vitro. TFIID was immunoprecipiated from the
702 phosphocellulose 1M KCl fraction using a highly specific anti-TAF4 antibody. After extensive
703 washing, buffer alone (ctl) or a 6-fold molar excess amount of the promoter DNA (i.e. *bax* or
704 *hdm2* DNA) along with either p53 or p53 plus TFIIA was loaded onto the resins containing
705 TFIID. TFIID co-complexes were obtained after extensive washes followed by an elution step
706 using a specific peptide against TAF4. (B) Schematic representation of the *bax* and *hdm2*
707 promoter DNA templates used in the assembly reactions. Relative positions of p53 response
708 elements (RE), the core promoter element TATA box, and transcription start site (TSS) within
709 both p53 target gene promoters are indicated respectively. Eluates of TFIID co-complexes
710 obtained from the assembly reactions as described in (A) were analyzed by 4-12% SDS-PAGE
711 (Invitrogen) and visualized by silver staining analysis.

712

713 **Figure 2. Single Molecule Total Internal Reflection Fluorescence (TIRF) Microscopy**
714 **analysis of Quantum dot-labeled TFIID binding of promoter DNA in vitro.** (A) Schematic
715 representation of an in vitro single molecule TIRF assay to monitor binding of quantum dot
716 (QD)-labeled TFIID to fluorescently labeled *bax* or *hdm2* promoter DNA in real-time. (B) Co-
717 localization analysis of Cy3/Cy5-labeled promoter DNA and QD-labeled TFIID. Representative
718 2D projection maps of single promoter DNA molecules (red) and single TFIID complexes
719 (green) are shown. The intensity of the green spot reflects the time TFIID binds that specific
720 location on the slide. Transient binding (~1-2") results in a dim green spot. A co-localization
721 threshold of 84 nm was set based upon our previous study (21). Yellow boxes represent co-

722 localized molecules. The numbers below the projection maps represent the percentage of DNA
723 molecules co-localizing with TFIID (i.e. number of DNA molecules co-localizing with
724 TFIID/Total number of DNA molecules in a field of view). Due to the minute co-localization
725 efficiency (1.3%) in the absence of p53, higher DNA densities were necessary to yield a
726 statistically significant number of binding events. 2D histograms of TFIID–promoter DNA
727 displacement define the number of TFIID complexes mapped within 200 nm of a DNA molecule
728 in a particular field of view. σ equals the standard deviation (in nm) of the 2D Gaussian fits of
729 the TFIID–promoter DNA displacement histograms. N_{DNA}= Total number of DNA molecules in
730 a field of view. (C) Dependence of TFIID/promoter DNA co-localization on p53, the p53 RE,
731 and core promoter elements. Promoter DNA binding is plotted as a percentage of total DNA
732 molecules in a field of view that are co-localized with TFIID over 15' of binding based on
733 TFIID–promoter DNA displacement histograms. TFIID binding to wild-type *bax* DNA is
734 compared with and without p53. Additional comparisons were made for TFIID binding to wild-
735 type (WT), Mutant p53 RE (Mu RE), Mutant Core (Mu Core), or combined mutant RE and core
736 (Mu RE/Co) *hdm2* DNA templates. (D) xlink-Exo analysis of TFIID binding to wild-type (top
737 panel) and Mu RE/Co (bottom panel) *hdm2* DNA. Basepair annotations (+/- 2bp) above
738 individual peaks in the line traces (right panel) represent a -4bp adjustment to reflect the known
739 inability of Exonuclease III to cut immediately adjacent to protein/DNA crosslink sites (32).
740
741 **Figure 3. Residence time analysis of TFIID bound to promoter DNA.** (A) Individual co-
742 localized TFIID/promoter DNA binding events were further analyzed to determine the average
743 residence time for TFIID bound to wild-type *hdm2* promoter DNA in the absence (left panel) and
744 presence (right panel) of p53. 1–Cumulative Distribution Function Plots (1–CDF) of TFIID
745 bound to DNA were fitted to a single (gray dashed) or two-component (red solid) exponential

746 decay model. Fitting analysis reveals that TFIID complexes bound to promoter DNA display
747 residence times comprised of a long- (τ1) and a short- (τ2) lived component. Percentages of the
748 long- (τ1) and short- (τ2) lived components are listed next to the residence time. (B) Average
749 residence time analysis for TFIID bound to Mu RE(left panel), Mu Core (middle panel), and Mu
750 RE/Co (right panel) *hdm2* promoter DNA in the presence of p53 as described in (A).
751
752 **Figure 4. Residence time analysis of p53 bound to promoter DNA with and without TFIID.**
753 (A) Individual co-localized p53/promoter DNA binding events were further analyzed to
754 determine the average residence time for p53 bound to wild-type (left panel) and Mutant p53 RE
755 (right panel) *hdm2* promoter DNA. 1−Cumulative Distribution Function Plots (1−CDF) of p53
756 bound to promoter DNA were fit to a single (gray dashed) or two (red solid)-component
757 exponential decay model. Based on comparisons of the *hdm2* promoter DNAs containing wild-
758 type and mutant p53 REs, τ1 represents specific binding of p53 to the wild-type *hdm2* DNA
759 while τns equals non-specific interactions between p53 and promoter DNA. (B) 1−Cumulative
760 Distribution Function Plot (1−CDF) of p53 bound to the wild-type *hdm2* DNA template in the
761 presence of TFIID was fit to a single (gray dashed) and two (red solid)-component exponential
762 decay (left panel) or gamma distribution (right panel) model. (C) Comparison of p53's residence
763 time (τ1) on the wild-type *hdm2* DNA with and without TFIID based upon the results shown in
764 (A) and (B) (left panel). Comparison of TFIID's and p53's residence time (τ1) on the wild-type
765 *hdm2* DNA based upon results shown in Figures 3 and 4.
766
767 **Figure 5. Structural EM analysis on p53's impact on TFIID bound to native target gene**
768 **promoters.** (A) TFIID's structural plasticity as defined by the position of its Lobe A (24)(top

769 panels, the major lobes of TFIID are labeled as A, B, and C). TFIID's conformations are
770 classified into three groups: Canonical, Transition and Rearranged state as shown. Reference-
771 free 2D classification analysis on negative stain EM datasets showing populations of different
772 TFIID conformations in the absence of p53 (gray), presence of p53 (white), and with p53 + *bax*
773 DNA (black). The scale bar represents 100Å. (B) Three representative reference-free 2D class
774 averages of p53/TFIID/TFIIA bound to either the *bax* or *hdm2* DNA are shown based upon cryo-
775 EM particle datasets. The scale bar is 200Å. (C) Distinct 2D class averages showing views of the
776 assemblies bound to the *bax* promoter DNA fragment downstream (top panel, DNA highlighted
777 in green arrows) and upstream (middle panel, DNA highlighted in yellow arrows) of the
778 transcription start site (TSS, +1) are presented respectively. The orientation of the core promoter
779 elements bound by TFIID were previously mapped in the 3D structure of TFIID/TFIIA bound to
780 the super-core promoter (SCP) DNA (24). The corresponding views of the 3D structure of
781 TFIID/TFIIA/SCP DNA are shown (far right) to indicate the DNA orientation. The strong 3D
782 density highlighted in green represents the promoter DNA comprising the initiator, TSS and
783 downstream promoter elements. Since the upstream promoter DNA was weakly visible, focused
784 classification analysis (bottom panel) were performed using those corresponding class averages
785 (middle panel) to clarify the presence of the *bax* promoter DNA upstream of the TATA box
786 (highlighted by yellow arrow). The scale bar is 200Å.
787
788 **Figure 6. A representative model of how p53 induces a common DNA binding mode**
789 **within TFIID that targets various p53-responsive promoters.**
790 A proposed model of how p53 facilitates a common structural module within TFIID for core
791 promoter recognition is presented based upon our current and previous studies (20). In the

792 absence of DNA, p53 binds to lobe A/C, which results in a shortening of the distance between
793 lobes A and B in addition to an extension of lobe D (20). This structural repositioning of lobe A
794 to lobe B results in the formation of a common DNA-binding mode within TFIID that allows
795 recognition of various p53 target promoters. Once TFIID structurally rearranges, p53 disengages
796 via loss of its contacts with Lobe A/C to allow TFIID to stably bind the promoter. Dissociation
797 of p53 from the TFIID/promoter DNA scaffold results in "recycling" of the p53 RE for further
798 assembly of the PIC components. The scale bar represents 100Å.
799
800
801

801 **References**

802 1. **Menendez D, Inga A, Resnick MA.** 2009. The expanding universe of p53 targets. Nat
803 Rev Cancer **9:**724-737.
804 2. **Bieging KT, Mello SS, Attardi LD.** 2014. Unravelling mechanisms of p53-mediated
805 tumour suppression. Nat Rev Cancer **14:**359-370.
806 3. **Tafvizi A, Huang F, Fersht AR, Mirny LA, van Oijen AM.** 2011. A single-molecule
807 characterization of p53 search on DNA. Proc Natl Acad Sci U S A **108:**563-568.
808 4. **Lu H, Levine AJ.** 1995. Human TAFII31 protein is a transcriptional coactivator of the
809 p53 protein. Proc Natl Acad Sci U S A **92:**5154-5158.
810 5. **Thut CJ, Chen JL, Klemm R, Tjian R.** 1995. p53 transcriptional activation mediated
811 by coactivators TAFII40 and TAFII60. Science **267:**100-104.
812 6. **Buschmann T, Lin Y, Aithmitti N, Fuchs SY, Lu H, Resnick-Silverman L, Manfredi**
813 **JJ, Ronai Z, Wu X.** 2001. Stabilization and activation of p53 by the coactivator protein
814 TAFII31. J Biol Chem **276:**13852-13857.
815 7. **Li AG, Piluso LG, Cai X, Gadd BJ, Ladurner AG, Liu X.** 2007. An acetylation switch
816 in p53 mediates holo-TFIID recruitment. Mol Cell **28:**408-421.
817 8. **Juven-Gershon T, Hsu JY, Kadonaga JT.** 2006. Perspectives on the RNA polymerase
818 II core promoter. Biochem Soc Trans **34:**1047-1050.
819 9. **Colgan J, Manley JL.** 1992. TFIID can be rate limiting in vivo for TATA-containing,
820 but not TATA-lacking, RNA polymerase II promoters. Genes Dev **6:**304-315.
821 10. **Chi T, Carey M.** 1996. Assembly of the isomerized TFIIA--TFIID--TATA ternary
822 complex is necessary and sufficient for gene activation. Genes Dev **10:**2540-2550.
823 11. **Wang W, Gralla JD, Carey M.** 1992. The acidic activator GAL4-AH can stimulate
824 polymerase II transcription by promoting assembly of a closed complex requiring TFIID
825 and TFIIA. Genes Dev **6:**1716-1727.
826 12. **White J, Brou C, Wu J, Lutz Y, Moncollin V, Chambon P.** 1992. The acidic
827 transcriptional activator GAL-VP16 acts on preformed template-committed complexes.
828 Embo J **11:**2229-2240.
829 13. **Chi T, Carey M.** 1993. The ZEBRA activation domain: modular organization and
830 mechanism of action. Mol Cell Biol **13:**7045-7055.
831 14. **Lieberman PM, Berk AJ.** 1994. A mechanism for TAFs in transcriptional activation:
832 activation domain enhancement of TFIID-TFIIA--promoter DNA complex formation.
833 Genes Dev **8:**995-1006.
834 15. **Chi T, Lieberman P, Ellwood K, Carey M.** 1995. A general mechanism for
835 transcriptional synergy by eukaryotic activators. Nature **377:**254-257.
836 16. **Kobayashi N, Boyer TG, Berk AJ.** 1995. A class of activation domains interacts
837 directly with TFIIA and stimulates TFIIA-TFIID-promoter complex assembly. Mol Cell
838 Biol **15:**6465-6473.
839 17. **Rhee HS, Pugh BF.** 2012. Genome-wide structure and organization of eukaryotic pre-
840 initiation complexes. Nature **483:**295-301.
841 18. **Lieberman PM, Ozer J, Gursel DB.** 1997. Requirement for transcription factor IIA
842 (TFIIA)-TFIID recruitment by an activator depends on promoter structure and template
843 competition. Mol Cell Biol **17:**6624-6632.

844 19. **Xing J, Sheppard HM, Corneillie SI, Liu X.** 2001. p53 Stimulates TFIID-TFIIA-
845 promoter complex assembly, and p53-T antigen complex inhibits TATA binding protein-
846 TATA interaction. Mol Cell Biol **21:**3652-3661.
847 20. **Liu WL, Coleman RA, Ma E, Grob P, Yang JL, Zhang Y, Dailey G, Nogales E,**
848 **Tjian R.** 2009. Structures of three distinct activator-TFIID complexes. Genes Dev
849 **23:**1510-1521.
850 21. **Revyakin A, Zhang Z, Coleman RA, Li Y, Inouye C, Lucas JK, Park SR, Chu S,**
851 **Tjian R.** 2012. Transcription initiation by human RNA polymerase II visualized at
852 single-molecule resolution. Genes Dev **26:**1691-1702.
853 22. **Liu WL, Coleman RA, Grob P, King DS, Florens L, Washburn MP, Geles KG,**
854 **Yang JL, Ramey V, Nogales E, Tjian R.** 2008. Structural changes in TAF4b-TFIID
855 correlate with promoter selectivity. Mol Cell **29:**81-91.
856 23. **Papai G, Tripathi MK, Ruhlmann C, Layer JH, Weil PA, Schultz P.** 2010. TFIIA
857 and the transactivator Rap1 cooperate to commit TFIID for transcription initiation.
858 Nature **465:**956-960.
859 24. **Cianfrocco MA, Kassavetis GA, Grob P, Fang J, Juven-Gershon T, Kadonaga JT,**
860 **Nogales E.** 2013. Human TFIID binds to core promoter DNA in a reorganized structural
861 state. Cell **152:**120-131.
862 25. **Louder RK, He Y, Lopez-Blanco JR, Fang J, Chacon P, Nogales E.** 2016. Structure
863 of promoter-bound TFIID and model of human pre-initiation complex assembly. Nature
864 **531:**604-609.
865 26. **Andel F, 3rd, Ladurner AG, Inouye C, Tjian R, Nogales E.** 1999. Three-dimensional
866 structure of the human TFIID-IIA-IIB complex. Science **286:**2153-2156.
867 27. **Grob P, Cruse MJ, Inouye C, Peris M, Penczek PA, Tjian R, Nogales E.** 2006. Cryo-
868 electron microscopy studies of human TFIID: conformational breathing in the integration
869 of gene regulatory cues. Structure **14:**511-520.
870 28. **Miyashita T, Reed JC.** 1995. Tumor suppressor p53 is a direct transcriptional activator
871 of the human bax gene. Cell **80:**293-299.
872 29. **Manfredi JJ.** 2010. The Mdm2-p53 relationship evolves: Mdm2 swings both ways as an
873 oncogene and a tumor suppressor. Genes Dev **24:**1580-1589.
874 30. **Bourdon JC, Deguin-Chambon V, Lelong JC, Dessen P, May P, Debuire B, May E.**
875 1997. Further characterisation of the p53 responsive element--identification of new
876 candidate genes for trans-activation by p53. Oncogene **14:**85-94.
877 31. **Juven-Gershon T, Cheng S, Kadonaga JT.** 2006. Rational design of a super core
878 promoter that enhances gene expression. Nat Methods **3:**917-922.
879 32. **Chang GS, Chen XA, Park B, Rhee HS, Li P, Han KH, Mishra T, Chan-Salis KY,**
880 **Li Y, Hardison RC, Wang Y, Pugh BF.** 2014. A comprehensive and high-resolution
881 genome-wide response of p53 to stress. Cell Rep **8:**514-527.
882 33. **Galasinski SK, Lively TN, Grebe De Barron A, Goodrich JA.** 2000. Acetyl coenzyme
883 A stimulates RNA polymerase II transcription and promoter binding by transcription
884 factor IID in the absence of histones. Mol Cell Biol **20:**1923-1930.
885 34. **Zhang Z, Boskovic Z, Hussain MM, Hu W, Inouye C, Kim HJ, Abole AK, Doud**
886 **MK, Lewis TA, Koehler AN, Schreiber SL, Tjian R.** 2015. Chemical perturbation of
887 an intrinsically disordered region of TFIID distinguishes two modes of transcription
888 initiation. Elife **4**.

889 35. **Mazur SJ, Sakaguchi K, Appella E, Wang XW, Harris CC, Bohr VA.** 1999.
890 Preferential binding of tumor suppressor p53 to positively or negatively supercoiled DNA
891 involves the C-terminal domain. J Mol Biol **292:**241-249.
892 36. **Weinberg RL, Freund SM, Veprintsev DB, Bycroft M, Fersht AR.** 2004. Regulation
893 of DNA binding of p53 by its C-terminal domain. J Mol Biol **342:**801-811.
894 37. **Emamzadah S, Tropia L, Vincenti I, Falquet B, Halazonetis TD.** 2014. Reversal of
895 the DNA-binding-induced loop L1 conformational switch in an engineered human p53
896 protein. J Mol Biol **426:**936-944.
897 38. **Floyd DL, Harrison SC, van Oijen AM.** 2010. Analysis of kinetic intermediates in
898 single-particle dwell-time distributions. Biophys J **99:**360-366.
899 39. **Phelps M, Darley M, Primrose JN, Blaydes JP.** 2003. p53-independent activation of
900 the hdm2-P2 promoter through multiple transcription factor response elements results in
901 elevated hdm2 expression in estrogen receptor alpha-positive breast cancer cells. Cancer
902 Res **63:**2616-2623.
903 40. **Gazit K, Moshonov S, Elfakess R, Sharon M, Mengus G, Davidson I, Dikstein R.**
904 2009. TAF4/4b x TAF12 displays a unique mode of DNA binding and is required for
905 core promoter function of a subset of genes. J Biol Chem **284:**26286-26296.
906 41. **Li AG, Piluso LG, Cai X, Gadd BJ, Ladurner AG, Liu X.** 2007. An acetylation switch
907 in p53 mediates holo-TFIID recruitment. Mol Cell **28:**408-421.
908 42. **Espinosa JM, Emerson BM.** 2001. Transcriptional regulation by p53 through intrinsic
909 DNA/chromatin binding and site-directed cofactor recruitment. Mol Cell **8:**57-69.
910 43. **Laptenko O, Shiff I, Freed-Pastor W, Zupnick A, Mattia M, Freulich E, Shamir I,**
911 **Kadouri N, Kahan T, Manfredi J, Simon I, Prives C.** 2015. The p53 C terminus
912 controls site-specific DNA binding and promotes structural changes within the central
913 DNA binding domain. Mol Cell **57:**1034-1046.
914 44. **Liu X, Berk AJ.** 1995. Reversal of in vitro p53 squelching by both TFIIB and TFIID.
915 Mol Cell Biol **15:**6474-6478.
916 45. **Espinosa JM, Verdun RE, Emerson BM.** 2003. p53 functions through stress- and
917 promoter-specific recruitment of transcription initiation components before and after
918 DNA damage. Mol Cell **12:**1015-1027.
919 46. **Okuda M, Nishimura Y.** 2015. Real-time and simultaneous monitoring of the
920 phosphorylation and enhanced interaction of p53 and XPC acidic domains with the
921 TFIIH p62 subunit. Oncogenesis **4:**e150.
922 47. **Xiao H, Pearson A, Coulombe B, Truant R, Zhang S, Regier JL, Triezenberg SJ,**
923 **Reinberg D, Flores O, Ingles CJ, et al.** 1994. Binding of basal transcription factor
924 TFIIH to the acidic activation domains of VP16 and p53. Mol Cell Biol **14:**7013-7024.
925 48. **Leveillard T, Andera L, Bissonnette N, Schaeffer L, Bracco L, Egly JM, Wasylyk B.**
926 1996. Functional interactions between p53 and the TFIIH complex are affected by
927 tumour-associated mutations. EMBO J **15:**1615-1624.
928 49. **Maston GA, Evans SK, Green MR.** 2006. Transcriptional regulatory elements in the
929 human genome. Annu Rev Genomics Hum Genet **7:**29-59.
930 50. **Huang B, Jones SA, Brandenburg B, Zhuang X.** 2008. Whole-cell 3D STORM reveals
931 interactions between cellular structures with nanometer-scale resolution. Nat Methods
932 **5:**1047-1052.

933 51. **Chen J, Zhang Z, Li L, Chen BC, Revyakin A, Hajj B, Legant W, Dahan M,**
934 **Lionnet T, Betzig E, Tjian R, Liu Z.** 2014. Single-molecule dynamics of enhanceosome
935 assembly in embryonic stem cells. Cell **156:**1274-1285.
936 52. **Ludtke SJ, Baldwin PR, Chiu W.** 1999. EMAN: semiautomated software for high-
937 resolution single-particle reconstructions. J Struct Biol **128:**82-97.
938 53. **Mastronarde DN.** 2005. Automated electron microscope tomography using robust
939 prediction of specimen movements. J Struct Biol **152:**36-51.
940 54. **Mindell JA, Grigorieff N.** 2003. Accurate determination of local defocus and specimen
941 tilt in electron microscopy. J Struct Biol **142:**334-347.
942 55. **Shaikh TR, Gao H, Baxter WT, Asturias FJ, Boisset N, Leith A, Frank J.** 2008.
943 SPIDER image processing for single-particle reconstruction of biological
944 macromolecules from electron micrographs. Nat Protoc **3:**1941-1974.
945 56. **van Heel M, Harauz G, Orlova EV, Schmidt R, Schatz M.** 1996. A new generation of
946 the IMAGIC image processing system. J Struct Biol **116:**17-24.
947 57. **Chen JZ, Grigorieff N.** 2007. SIGNATURE: a single-particle selection system for
948 molecular electron microscopy. J Struct Biol **157:**168-173.
949 58. **Lander GC, Stagg SM, Voss NR, Cheng A, Fellmann D, Pulokas J, Yoshioka C,**
950 **Irving C, Mulder A, Lau PW, Lyumkis D, Potter CS, Carragher B.** 2009. Appion: an
951 integrated, database-driven pipeline to facilitate EM image processing. J Struct Biol
952 **166:**95-102.
953 59. **Pettersen EF, Goddard TD, Huang CC, Couch GS, Greenblatt DM, Meng EC,**
954 **Ferrin TE.** 2004. UCSF Chimera--a visualization system for exploratory research and
955 analysis. J Comput Chem **25:**1605-1612.
956

Figure 1

Coleman_Fig. 1

A

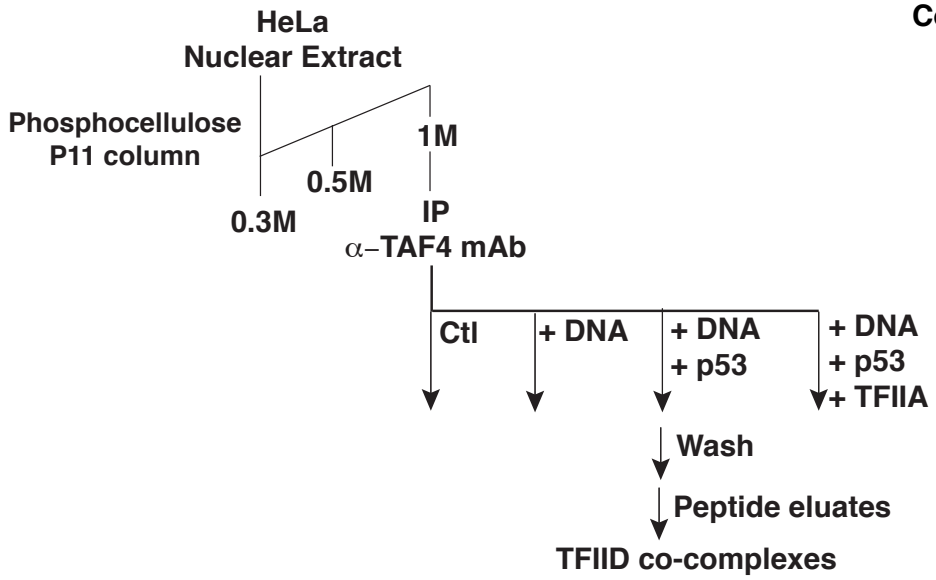

B

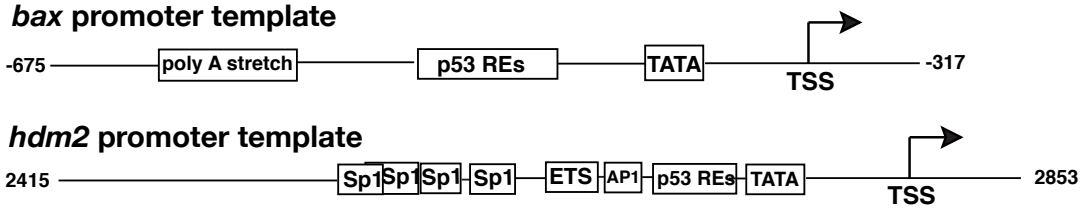

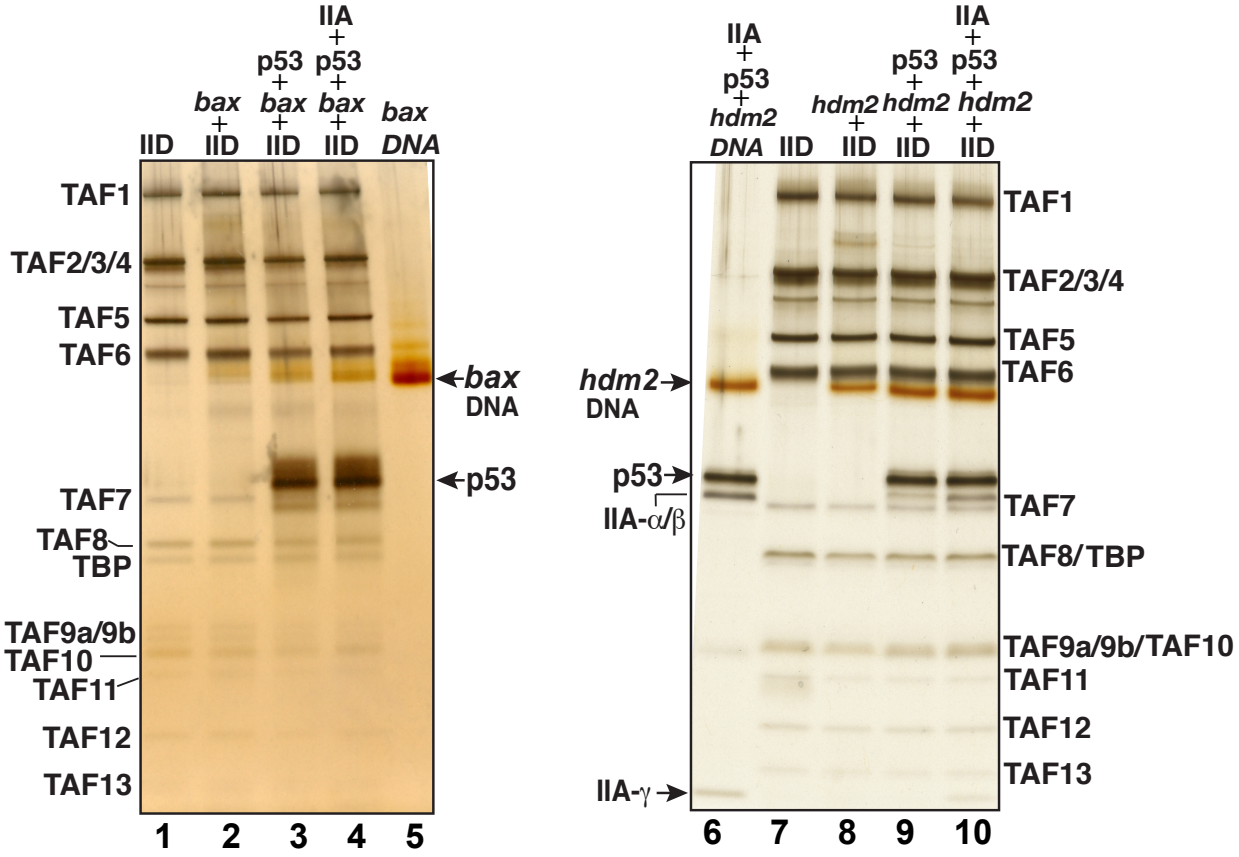

Figure 2

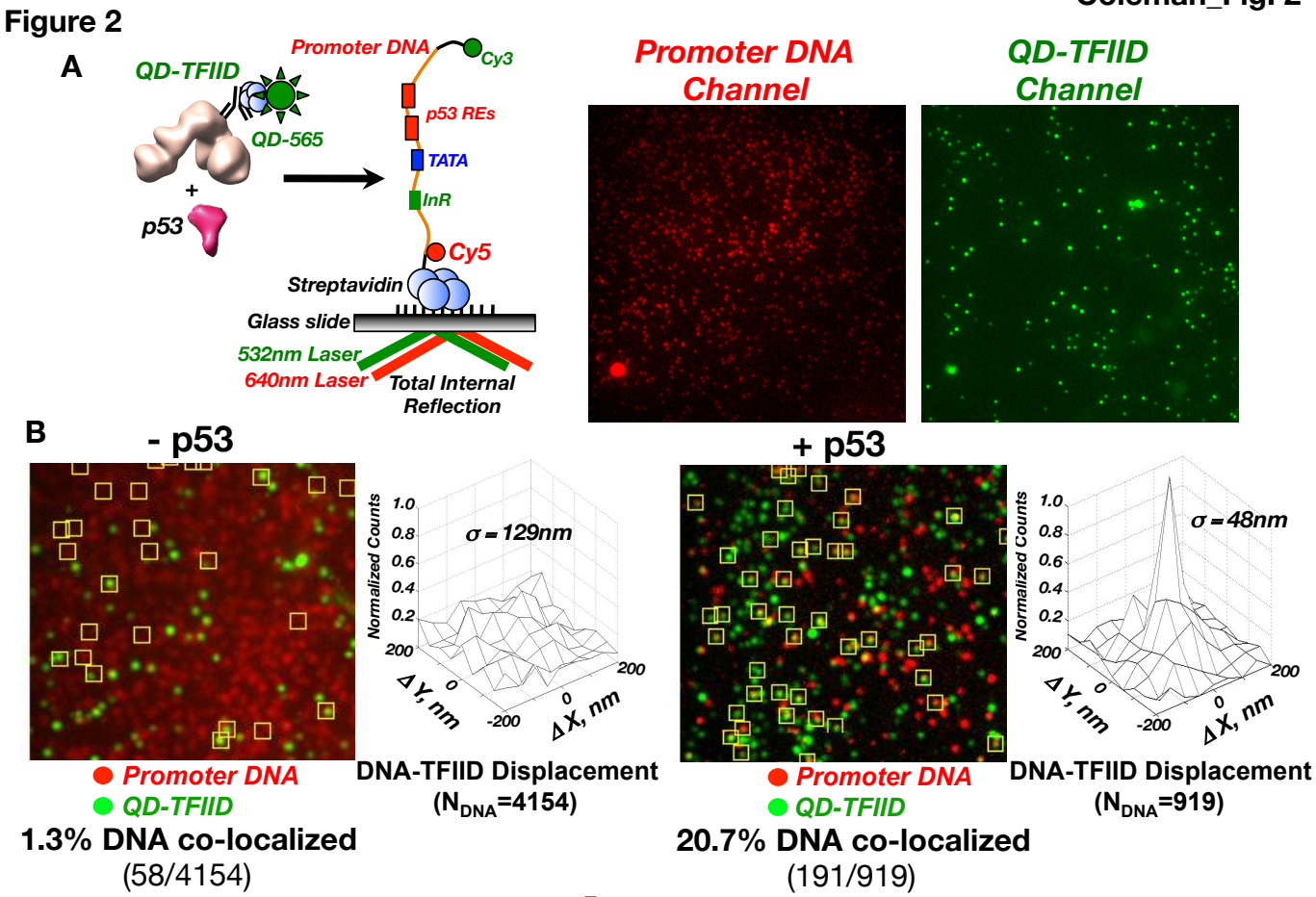
A
QD-TFIID
QD-565
p53
Promoter DNA
Cy3
p53 REs
TATA
InR
Cy5
Streptavidin
Glass slide
532nm Laser
640nm Laser
Total Internal Reflection
Promoter DNA Channel
QD-TFIID Channel
B
- p53
σ = 129nm
Normalized Counts
ΔY, nm
ΔX, nm
Promoter DNA
QD-TFIID
DNA-TFIID Displacement
(N_DNA=4154)
1.3% DNA co-localized
(58/4154)
+ p53
σ = 48nm
Promoter DNA
QD-TFIID
DNA-TFIID Displacement
(N_DNA=919)
20.7% DNA co-localized
(191/919)

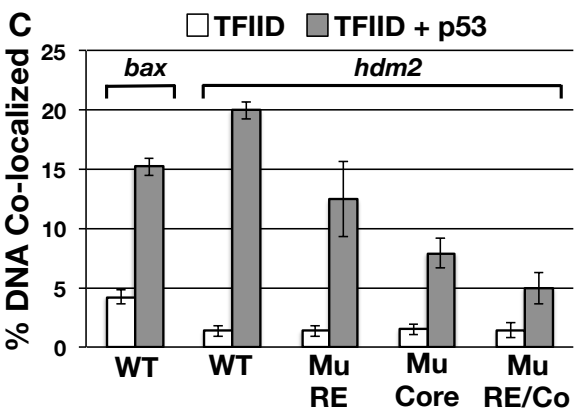
C
TFIID
TFIID + p53
% DNA Co-localized
bax
hdm2
WT
WT
Mu RE
Mu Core
Mu RE/Co

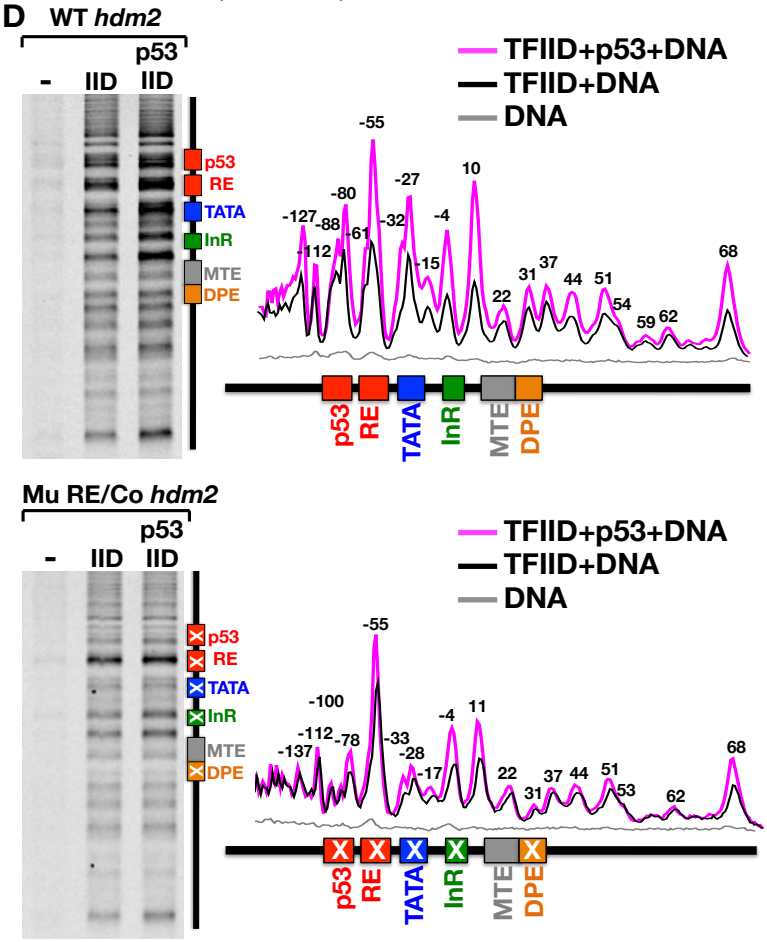
D
WT hdm2
-
IID
p53 IID
p53
RE
TATA
InR
MTE
DPE
TFIID+p53+DNA
TFIID+DNA
DNA
Mu RE/Co hdm2

Coleman_Fig. 3

Figure 3

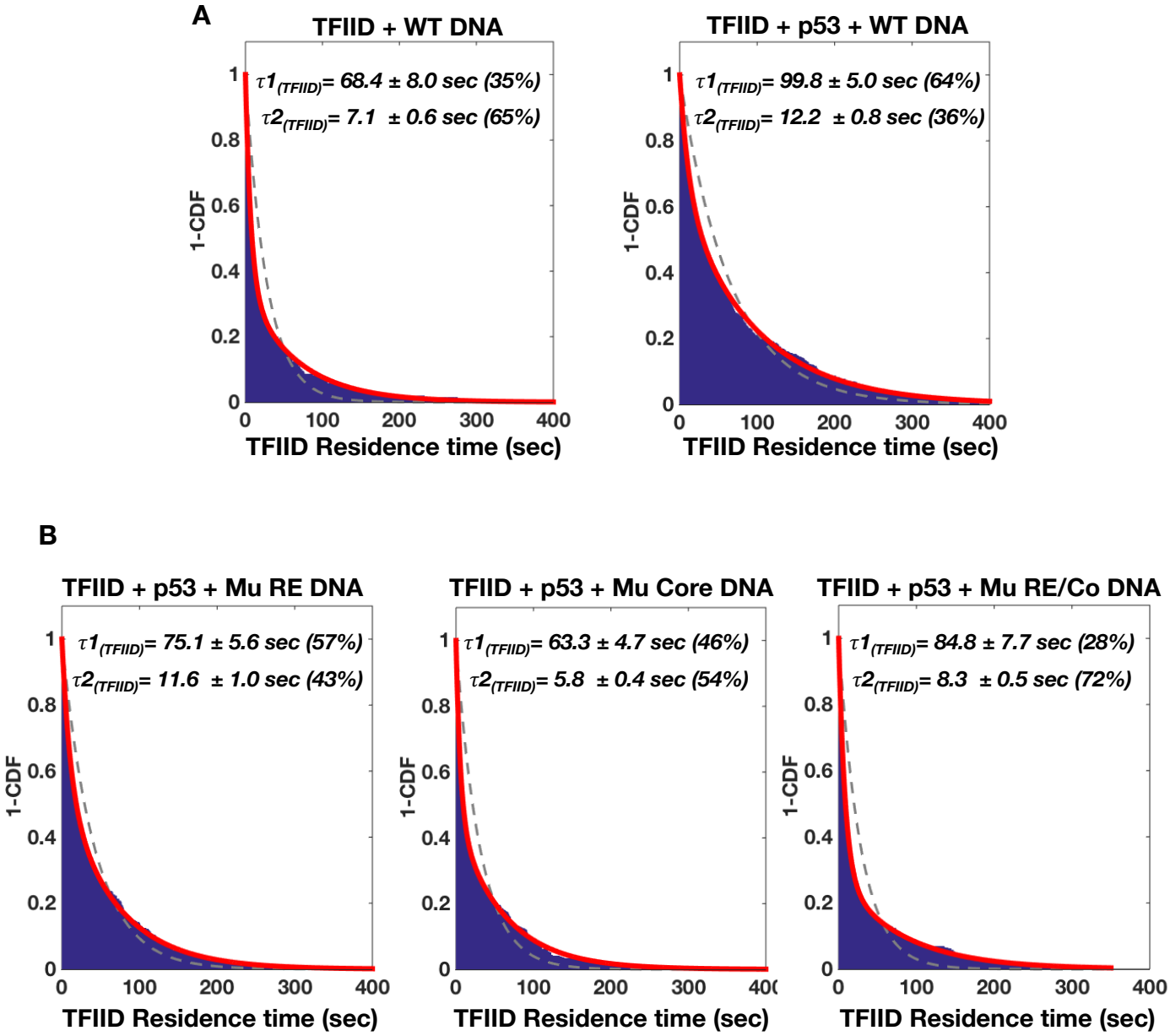

Figure 4

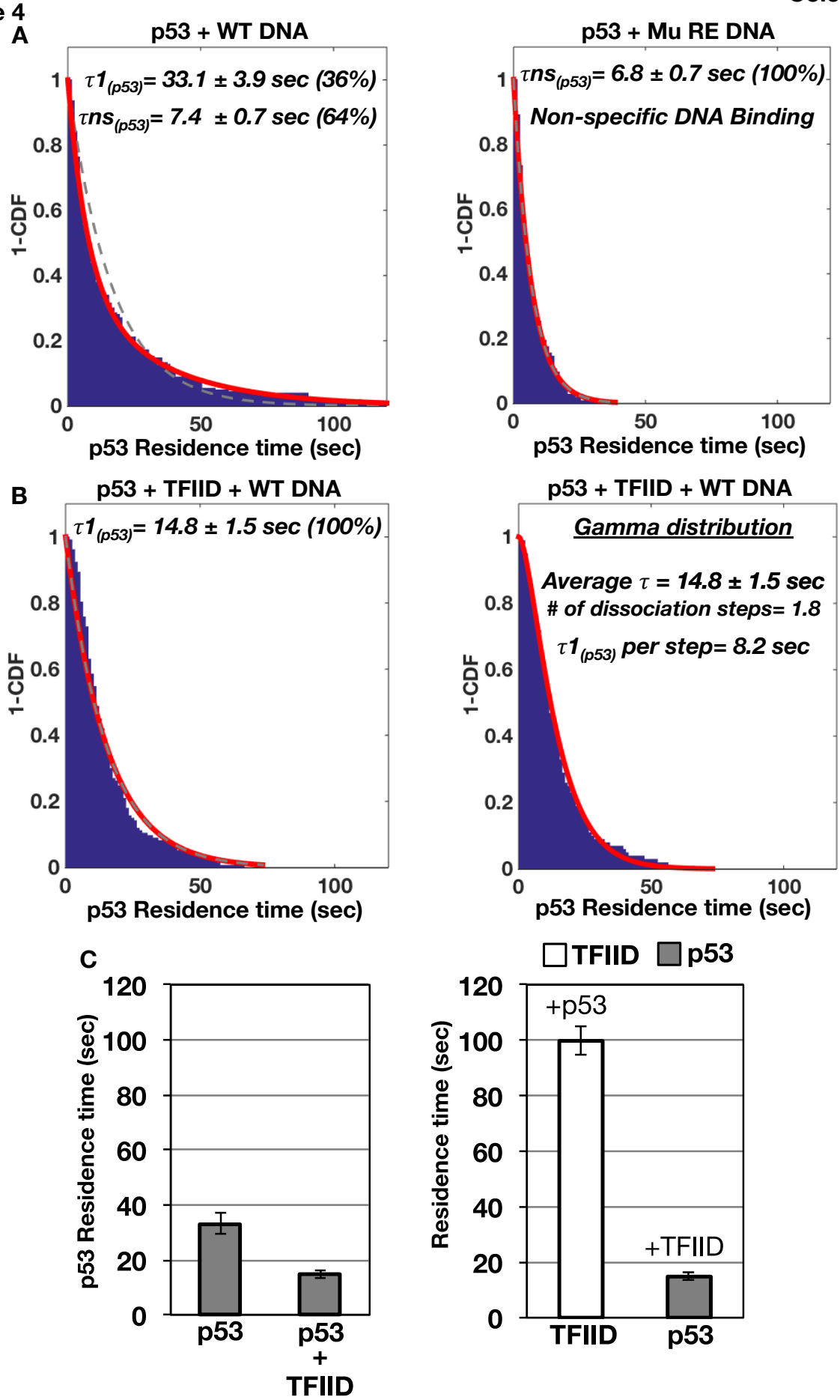
A
p53 + WT DNA
τ1(p53)= 33.1 ± 3.9 sec (36%)
τns(p53)= 7.4 ± 0.7 sec (64%)
1-CDF
p53 Residence time (sec)
p53 + Mu RE DNA
τns(p53)= 6.8 ± 0.7 sec (100%)
Non-specific DNA Binding
B
p53 + TFIID + WT DNA
τ1(p53)= 14.8 ± 1.5 sec (100%)
Gamma distribution
Average τ = 14.8 ± 1.5 sec
# of dissociation steps= 1.8
τ1(p53) per step= 8.2 sec
C
p53 Residence time (sec)
p53
p53 + TFIID
TFIID
p53
Residence time (sec)
+p53
+TFIID

Figure 5

Coleman_Fig. 5

A

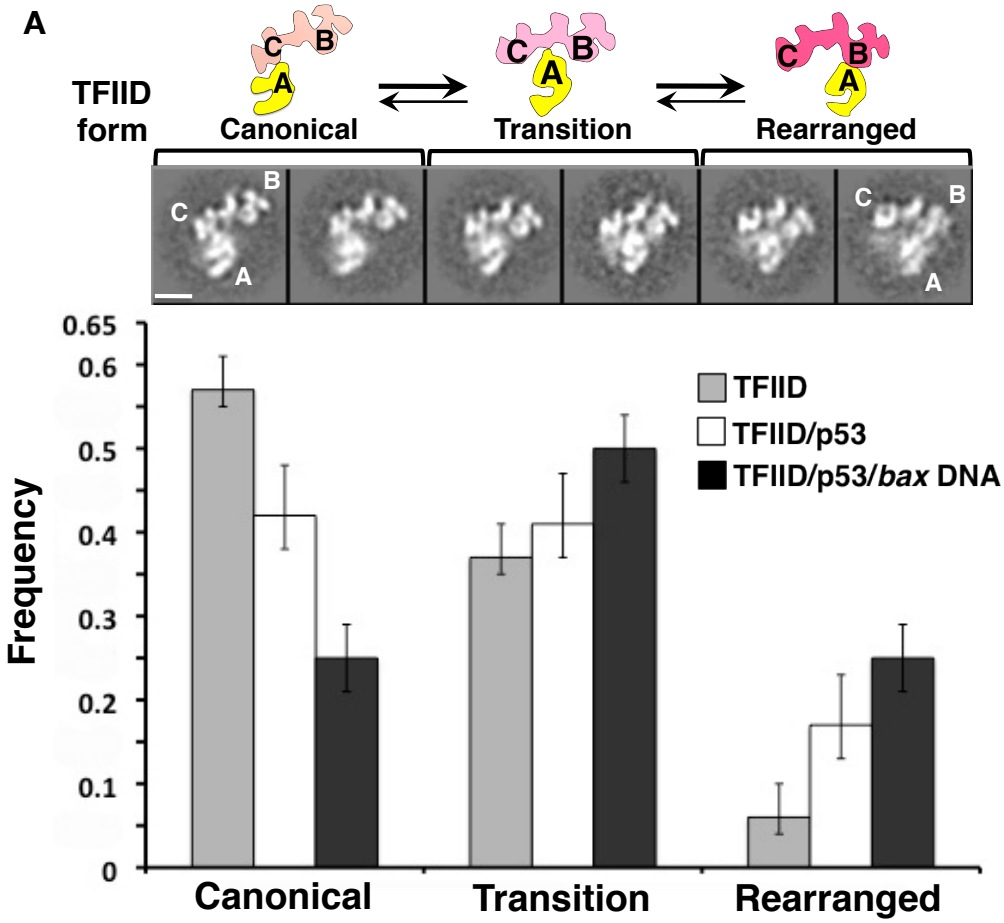

B

TFIID/p53/TFIIA/promoter DNA

bax promoter

hdm2 promoter

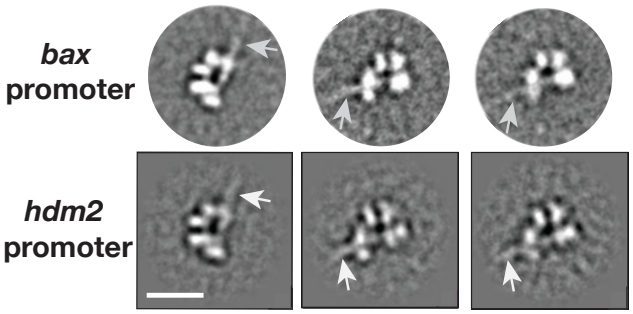

C strong downstream DNA view

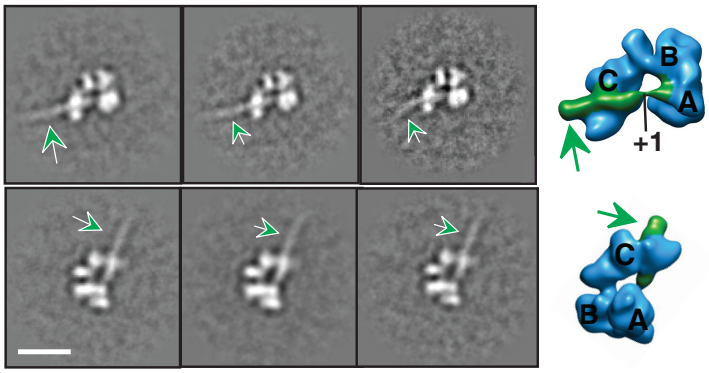

weak upstream DNA view

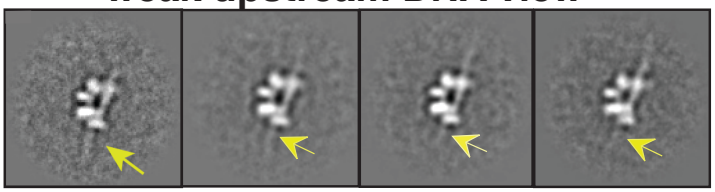

Focused classification: upstream DNA

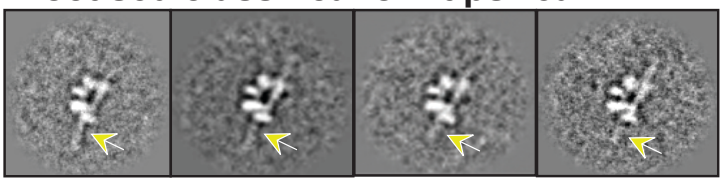

Figure 6

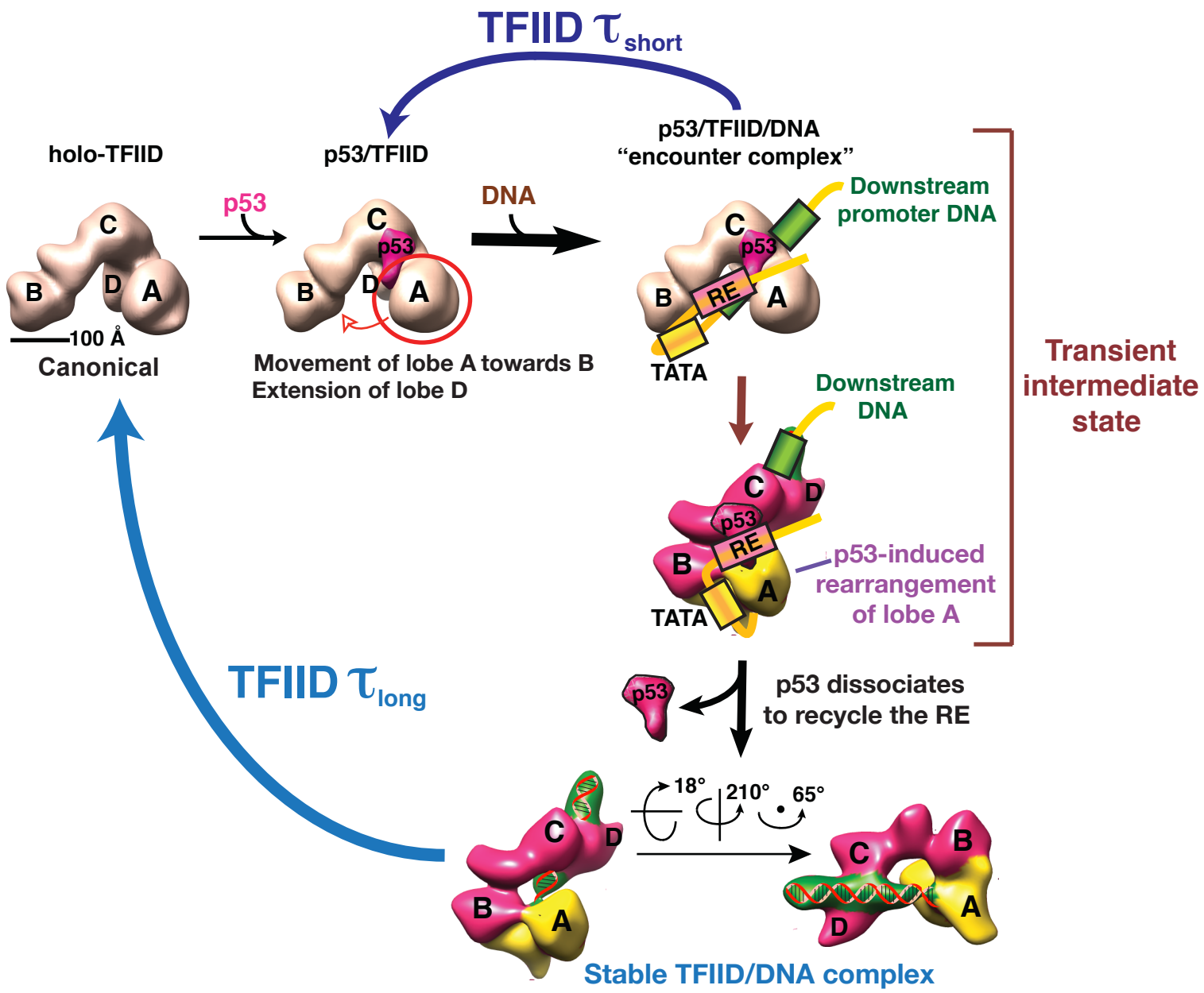
TFIID τshort
holo-TFIID
p53/TFIID
p53/TFIID/DNA
"encounter complex"
p53
DNA
Downstream promoter DNA
C
B
D
A
100 Å
Canonical
p53
Movement of lobe A towards B
Extension of lobe D
RE
TATA
Downstream DNA
p53-induced rearrangement of lobe A
Transient intermediate state
TFIID τlong
p53 dissociates to recycle the RE
18°
210°
65°
Stable TFIID/DNA complex